J Math Chem (2013) 51:1479–1514
DOI 10.1007/s10910-013-0159-2

REVIEW

Reflections on the conformation, topology and thermodynamics of a polyelectrolyte chain in the presence of counterions with plausible applications

C. G. Jesudason · A. J. P. Agung

Received: 7 January 2013 / Accepted: 8 March 2013 / Published online: 11 April 2013

Abstract The simulation results from a basic polyelectrolyte chain consisting of an anionic string of 150 univalent negatively charged particles connected under various harmonic-like potential interactions with each other in the presence of a similar number of positive and free counter ions found in Jesudason et al. (EPJE 30:341–350, 2009) forms the focal point for further discussion on chain models based on a survey of more recent developments in general polyelectrolyte theory. The topics discussed include persistence length definition, forcefields and methods of controlling simulation parameters, and thermodynamics. The data for the basic system was derived for the temperature range 0.1–10.0 in reduced units (corresponding to $\xi = 10$–0.1); the augmented data involves a 360 monomer chain. The data include the total and Coulombic energies, radial distribution functions, radii of gyration, end-to-end distances and snapshots of the system which are all discussed anew. Polyelectrolyte systems have been overwhelmingly associated with biophysical interpretations, but here it is suggested that these detailed studies and the consequent theoretical formulations could be extended further afield; non-biological ionic liquid systems with catalytic and energy

C. G. Jesudason (✉)
Chemistry Department, Science Faculty, University of Malaya, Pantai Valley,
50603 Kuala Lumpur, Malaysia
e-mail: jesu@um.edu.my

C. G. Jesudason
Atomistic Simulation Centre, School of Mathematics and Physics, Queen's University
Belfast, Belfast BT7 1NN, Northern Ireland, UK
e-mail: c.jesudason@qub.ac.uk

A. J. P. Agung
Sumatera Institute of Technology (ITERA), Kota Baru Lampung South, Lampung Province,
Sumatera, Indonesia
e-mail: aang_agung@yahoo.com

storage applications are some of many other possibilities. However, the approach used by MD simulations to validate ionic liquid systems as carriers of molecules with catalytic moieties often refer to CPMD and DFT quantum methods, which is not the current norm as judged by the literature in especially coarse grained polyelectrolyte MD. The quantum approach could also be used for more detailed analysis of biophysical systems where one trend seems to be that the incorporation of details in simulations accounts for phenomena not explicable in coarser grained MD, for instance if conventional atomic ionic charges are assigned to all atom modeling. This is illustrated by a linear chain modeling a DNA polymer using different charge and size assignments for the same linear charge density. The trends are such that it might be expected that some form of routine standardization of force fields in the spirit of the Jorgensen OPLS-AA method that incorporates quantum calculations specific to a system will be implemented as a routine as refinements are seen to lead to more comprehensive rationalization.

Keywords Molecular dynamics simulation · Polyelectrolytes · Conformational studies

Mathematics Subject Classification (2000) 65P10 · 82B30

1 Introduction

Here we interpret the results [1] of a basic polyanionic chain MD simulation in terms of further consequent work[2] and other pertinent literature. Much of the computations concerning polyelectrolyte systems over the last decade seem to primarily concentrate on specific models with a view of rationalizing properties observed in real systems e.g [3,4,6,5,7–29]. In a rather comprehensive Perspective article on electrostatic (ES) force interactions [3], with a passing mention of electrodynamical forces e.g. London-type forces [30, p. 1892] and hydration and entropic forces [31], one is drawn to the general impression that whenever there is an extension to detail of the model [3, see esp. Sect. 2] an accounting for some basic phenomenon can be made. For instance, the forces between two long parallel double-helical macromolecules was elucidated only about 1997 by Kornyshev and Leikin [24]. Such an elucidation of the force fields (ff's) lead to the realization that the counter-ion condensation occurs along the grooves of the DNA strands. This in turn leads to the formulation of a force law due to the electrical double layers formed by mobile counterions and the charge imbalance. Such resultant interactions can then rationalize the fixed ('discrete') number of cation adsorbed cations, sequence specific pattern of twist angles for adjacent bp's, soliton -like DNA twist deformations, and other phenomena linked to the potential variation [3, p. 9944]. This further developed interaction energy

$$E(R, L) \approx L[a_0(R) - a_1(R)\cos\delta\phi + a_2(R)\cos 2\delta\phi] \tag{1}$$

of a DNA duplex of length L at perpendicular distance R with azimuthal frustration angle $\delta\phi$ has a coefficients that is a function of both f, the partition coefficient of cations in the major grooves and θ, the overall charge compensation fraction that

allows for consideration of charge distributions involving Donan equilibrium; a major challenge for this model, even for its detailed complexity is to account for water structuring in terms of hydration shells about the DNA [3, p. 9945, last paragraph]. Here we observe that this challenge would point to further detailed refinement. Currently, the force laws for these refinements tend to resort to solutions of the linearized Poisson–Boltzmann (PB) theory with specified or imposed boundary conditions [3, ref.151] and [5] with modified screening parameters (κ_k and κ_k^c for the screening inside and outside the rod modeled for persistence length calculations). These modifications lead to departures from the DH potentials [5, Figs. 1–2] which in the main is PB derived. Indeed, in most instances, the PB equations are deemed appropriate [25, p. 953], and for regions away from layers or surfaces where $\mid eq\varphi \geq k_bT \mid$, the PB equation reduces to the DH equation

$$\nabla^2\varphi(\mathbf{r}) = -4\pi\rho_{ext}(\mathbf{r})/\epsilon + \kappa_D^2\varphi(\mathbf{r}) \tag{2}$$

which is routinely utilized [25, p. 954] directly with the usual screening length parameter $\lambda_D = 1/\kappa_D$ where $\lambda_D = \left(4\pi l_B \sum_i n_i q_i^2\right)^{-1/2}$ is the usual screening length and this DH form is very effective not least because of compensating effects due to finite ion size [25, p. 954, par. after eqn. 33]. In line with the above substantiation, the interactions of DNA with proteins and histone NCP units are centered about these PB force fields with due modifications due to *structural details* [3, p. 9958]. Notwithstanding the discussion in [1, p. 341, Introduction] concerning the shortcomings of DH potentials to account for chain collapse or possible phase transitions, the highly developed techniques of mean field PB theories were used to account for some aspects of chain collapse [4] via dipole-dipole and correlation-induced electrostatic interactions. These dipoles are orthogonal to the tangent line of the polymer contour length and summation of the interactions stochastically over the entire length lead to the net attractive force. It appears that the theory follows the suggestion provided by Winkler et al. [22, last sentence]. The average interaction energy has the form

$$\left\langle E_{DD}(r) = \frac{-p^4 \exp^{-2\kappa r}}{4r^6\epsilon^2 k_B T} \right\rangle \tag{3}$$

where the screening parameter is κ. The proximity of the charges to form the dipole for an overall neutral system would invite comments concerning the use of the screening parameter and some follow below. The long range screened PB force fields are also used for modeling the attractive forces between two helical DNA's [24], which seems very reasonable, as with modeling of NCP attraction mediated by DNA [6] featuring the κ screening term, in conjunction with increasing details of the system, which implies solving the classical PB equations with the boundary conditions consonant with the additional details. Such solutions can give insight into general structure. Given the fact that a 2π azimuthal rotation between 2 DNA molecules vertically aligned leads to successive minima in the potential, such strips of charge on the DNA linked to the NCP's imply that the mutual azimuthal orientations of neighboring NCP's will alternate by $\approx \pi/4$ (Eq. 1, p. 11434); this is in fact the major prediction in [6]. These studies are carried out in conjunction with the availability of high resolution images

of these structures, which again illustrates the trend towards incorporating details derived from experiment with various standard ff's, in particular the PB formulation. The references above point to a very large literature and incremental research program over several decades; here we review results due to simulations of a polyelectrolyte chain [1,2] with the brief survey above serving as a background referring to some aspects of the following:

i. Determination of variables such as the bending constant in MD
ii. Review and derivation of persistence length expressions different from that of Manning, OSF and Dobrynin
iii. Reconstruction of thermodynamic equation of state and comment on κ for PB derived potential equations
iv. Elementary considerations in topology that suggests applications to not only catalysis, but to the construction of scaffolding and molecular structures, and to energy storage systems due to the very large ES energies
v. Since progress in biophysical studies seems to be related to the incorporation of structural details to models, it may be anticipated that the simulation protocols used in ionic liquid (IL) and other complex non-biological systems studies to derive molecular parameters directly from quantum chemical calculations for MD simulations would be extended to polyelectrolytes, in particular the charge distribution and the use of non-symmetrical force fields. With increasing computer power, one might anticipate that quantum chemical MD (such as CPMD) would become the preferred MD technique.

The earlier work [1] provides a broad and detailed survey of theoretical methods that are used to rationalize polyelectrolytes interactions; here we present the augmented data in relation to snapshots, providing suggestions of other possibilities not covered in [1], in addition to some other follow-up work [2]. Previously, much work centered mainly about mixed multi-charged (i.e. charges that were both positive and negative) polymer strands with counterions e.g. [32–34]. In these studies, the so-called screen Coulomb potential, also known as the Debye-Huckel potential of form $U^{DH} = l_B kT \frac{q_1 q_2 \exp(-\kappa r)}{r}$ were utilized. Such potentials are considered realistic in "weak" electrolyte solutions and certain possible phase transition phenomena such as reported here for a non-mixed charged polymer skeleton does not arise from such interactions. Other examples of conformational studies utilizing the screened Coulomb potential refer to the orientational correlation function [35]. These studies tend to focus on different charge configurational arrangements at constant temperature. Here the configuration is fixed and the temperature is the free variable in the simulations. The closest models to the current work aimed at free energy and entropy elucidations involve entropic sampling with a view of deriving thermodynamical properties via Ω , the system density of state from Monte Carlo moves in coordinate space [29,36,37]. Here the modified equations to the equation of state is quoted [2, eqn. 4.13, 4.14]. In particular, Klos and Pakula [37] examines some features related to the structure of these polyelectrolytes on a f.c.c lattice using Monte Carlo moves as with the others but uses an approximation to the Ewald summation method for electrostatic interactions. The physical shape for instance of the end-to-end distances is not as sharp as what is obtained here, and details in terms of RDF's were unfortunately not pro-

vided. The majority of mathematical treatments resort to solutions of the PB equations and its various approximations, such as the linearized Debye-Huckel (DH potential) as a solution [24,25]. The cornerstone for the successful application of this method is the existence of ρ, the charge density. This quantity is made available through the supporting electrolyte counter-ions, that are the main representations of the density due to their smallness in terms of both mass and size, leading to a highly mobile species. The small size implies that in setting up boundary conditions, the surface radii of these ions can often be neglected when compared to the NCP and DNA or polyelectrolyte strand. Obviously, with the breakdown of this approximation, counterion size and other charge-inducing effects would assume importance. At this level of refinement, however, one would be entering into the quantum realm of analysis, and this is not yet the main focus of polyelectrolyte simulation which seems to be heavily dependent on using the PB approximation in analysis with a few modifications to account for such size effects, where the analysis is essentially classical electrostatic analysis with some addition of dispersive force fields. For what follows, a classical force-field with dispersion forces modeled after the Lennard-Jones variety would be the main background assumptions, together with the validity of the PB-type equations for modeling charge distributions about larger and more strongly charged entities like the DNA polymer and NCP particles. Hybrid rationalizations too are possible, where counter-ions are considered in terms of dipole-dipole attractive interactions to account for the collapse of the polyelectrolyte [4]. Comments on some of these mechanisms follow.[1]

2 Model, method and parameters

The model for [1] consisted of 150 bonded particles (360 in [2]), where each particle represented the net charge of the repeat unit of the helix. The particles are connected by a harmonic potential U^h of the form listed below simulating a bond (5) and a bending potential U^b, (6). All particles interacted with the Φ_{LJ} potential with parameters depending on particle type. Details are described in [1] as are the number of runs, and nature of the equilibration process and sampling process. The pertinent force-fields and thermostats are described below. The computer simulation involved programming a TCl script which drives a C based MD code named ESPResSo [38] in an NVT ensemble. All ions interacted with the U^{C-P3M} potentials. The pertinent parameters and potentials for the interactions are defined as follows:

1. Non-bonded non-Coulombic Lennard-Jones potential Φ_{LJ}:

$$\Phi_{LJ} = 4\epsilon \left(\left(\frac{\sigma}{r-o}\right)^{12} - \left(\frac{\sigma}{r-o}\right)^{6} + s \right) \tag{4}$$

where o is the offset, s the shift parameter, σ the distance parameter, r the coordinate distance and ϵ the energy parameter.

[1] I am grateful to a reviewer for emphasizing the role of the counterions that is sometimes neglected in PB theory analysis.

2. Bonded interactions

(i) Harmonic potential U^h

$$U^h = \frac{k_h}{2}(r - R_H)^2 \tag{5}$$

where k_h is the force constant and R_H is the "equilibrium" length between two nuclear centers P_i and P_{i+1}.

(ii) Bending mode interaction potential U^b

$$U^b = \frac{k_b}{2}(\phi - \phi_0)^2 \tag{6}$$

Consider the three consecutive bonded centres P_i, P_{i+1} and P_{i+2}. Define the angle ϕ as the acute angle which can range from 0 to π ($\pi \leq \phi \geq 0$) between the lines $\overrightarrow{P_i P_{i+1}}$ and $\overrightarrow{P_i P_{i+2}}$. Similarly define ϕ_0. Then for nonzero k_b, the interaction for $\phi_0 = 0$ corresponds at zero temperature to the situation of the formation of a rod-like linear structure of the particles P_i linked together for maximum extension, whereas setting $\phi_0 = \pi$ corresponds to a chain collapsing on itself for any equilibrium bond length R_h. Hence these two selections form an envelope encompassing the entire range of interactions.

3. Non-bonded Coulombic interactions with potential U^{C-P3M}
The standard Coulombic potential may be written in the form

$$U^{C-P3M} = l_B kT \frac{q_1 q_2}{r} \tag{7}$$

where the Bjerrum length l_B is defined as $l_B = \frac{e^2}{4\pi\varepsilon_0\varepsilon_r k_B T}$ with the standard assignment of variables $\{e, k_B, T, \varepsilon_0, \varepsilon_r\}$ being the electronic charge, Boltzmann constant, Kelvin temperature, permittivity in vacuum and relative dielectric permittivity respectively. However (7) is computed in the Molecular Dynamics (MD) cell using the so called P3M technique [39] with an error tolerance in the total electrostatic energy less than tol_{err} for a series of random configurations, typically about 16 or more by adjusting or tuning the parameters connected to the method.

Thermostatting was carried out by the so called "Langevin" thermostat which has been described [40]; this method implies a synthetic algorithm where the equation of motion of the system Hamiltonian is modified to a form [40, eq. 8]

$$m_i \dot{v}_i = F_i + m_i \gamma \left(\frac{T_0}{T} - 1\right) v_i \tag{8}$$

where γ is an arbitrary coupling parameter, and T the instantaneous temperature determined from the kinetic energy. To compare with previous results and theories for fixed length chains [29,36], the chain length was kept constant to within 10 %

by scaling k_h with temperature. The computations in [29,36] have a maximum chain length of 81, and larger chain lengths seem to improve the statistics without introducing new phenomena and phase transitions. Here we have extended the length to 150 in [1] and 360 in [2]. If the extension from the equilibrium position of the Harmonic potential is x, then equipartition gives for a canonical coordinate x, $\langle x^2 \rangle = \frac{k_B}{k_h} T$. Assuming a loose validity of equipartition for the bond-distances, a large k_h was chosen and $k_h = 100T$ to ensure constancy of $\langle x^2 \rangle$. A more exact setting algorithm is described below. This setting to preserve overall length is required to correlate with theories for flexible non-extensible strings (e.g. in connection to persistence length and distance correlation length theories). In work [2], a more exact algorithm was developed for determining k_h and R_H which balances the Coulombic and harmonic forces [2, p. 14–17, Fig. 2.4]; clearly the method can be extended to higher order. The general average equilibrium criterion is

$$\begin{aligned} \mathbf{F}_{Total}(b, \Omega) = \mathbf{F}_{harmonic}(b, \Omega) + \mathbf{F}_{bending}(b, \Omega) + \mathbf{F}_{LJ}(b, \Omega) \\ + \mathbf{F}_{Coulomb}(b, \Omega) = 0 \end{aligned} \tag{9}$$

where b is the bond length ($b = R_H$ at equilibrium), Ω are the other independent thermodynamical parameters relevant to the problem and the $\mathbf{F}$'s are the forces associated with the variable indicated by the subscript. The approximation made here is that the forces between two adjacent monomers are sufficient, especially for systems that have significant screening. Hence, $\mathbf{F}_{bending} = 0$ and $\mathbf{F}_{Coulomb}$ and $\mathbf{F}_{LJ}$ are computable. Equating the forces at position b leads to a known function Φ [2, eqn. 2.14]

$$\Phi(k_h) = r(R_H = r \quad \text{at equilibrium}) \tag{10}$$

The energy of the adjacent polymer units at distance r, $U(r)$ is a known function as these are all defined in the ff's. For a fixed temperature, the only unknown is k_h (from 10) where

$$\bar{r}(k_h) = \frac{\int_0^\infty r \exp^{-U(r)/k_B T}\, dr}{\int_0^\infty \exp^{-U(r)/k_B T}\, dr} \tag{11}$$

for equal degeneracies over all r.The integral of (11) involves complicated Γ functions but one can evaluate $\bar{r}(k_h)$ numerically. From physical considerations, as $k_h \to \infty$, , $\bar{r} \to R_H$. The evaluation of (11) ([2, Fig. 2.4] leads to a graph with a very pronounced and sharp convergence of $\bar{r}$ to R_H for $k_h \geq 2,500$ and the lowest value is chosen to avoid computational singularities and overflows that would result from higher values. Exhaustive runs at salt concentrations 0–100 mM shows a maximum departure of the total contour length and average bond length of less that 0.1 % with a faintly perceptible decrease in value at higher salt concentration that can be attributed to screening, leading to a net attractive force between adjacent monomers [2, Figs. 2.5(a–b)]. This should be compared to the scaling used with temperature in [1] of 10 % rms fluctuation and the absolute setting for all runs of $k_h = 5000\epsilon_{LJ}/I_0^2$; $I_0 =$ bond length [21,22].

To ensure constancy of the Coulomb interaction, the Bjerrum parameter in (7) was scaled according to $l_B = 1./T$. If ξ, the reduced charge density parameter which reflects the strength of the polyionic charge is defined as $\xi = l_B/R_H$, then $\xi = 1/(TR_H)$. For [1], $\sigma = \epsilon = 1, o = 0, s = 1/4$ and Φ_{LJ} was cut-off at $r_{cut} = 2^{1/6}\sigma$ (= 1.12246) and the tolerance for the electrostatic energy was set at 10^{-6} reduced units. In the other more extended treatment [2], consisting of 360 monomer units in the chain, with 12 NCP particles and salt concentration set at the range 0.0-100mM of fully dissociated NaCl [2, p. 7], the Bjerrum length was set to 7.13 Å at temperature 300 K corresponding to the water solvent dielectric. For the runs in [2], the parameters in (4) are as follows which are scaled to correspond to the following real parameters, where σ = soft core radii, o = sum of hard core radii, s = constant s.t. $\Phi_{LJ} = 0$ at distance r_{cut} where $r_{cut} = 2^{1/6}\sigma$. The parameters for this potential for [2] is scaled such that they represent the following real values in the following format: {Parameter, DNA monomer, NCP, Na, Cl}, where {Radius (Å), 10.0, 35.0, 2.0, 2.0}, {Soft core radius (Å), 2.0, 2.0, 2.0, 2.0} {Hard core radius (Å), 8.0, 33.0, 0.0, 0.0}{Charge(e), −12, +150, +1, −1} {Mass (10^{-26} kg), 612.62, 18026.68, 3.819, 5.889} {Mass (reduced unit), 160.41, 4270.26, 1.0, 1.54}. For the simulation with 360 monomer units, the bending constant k_θ ($\equiv k_b$) was set by using the formula $k_\theta = L_p k_B T/b$ for all runs in [2], where b is the bond length and L_p the persistence length.

Four cases were investigated, Case(1–4) which had the following characteristics for the polyanionic skeleton:

Case 1 No bending mode vibrations (6), with electrostatic interactions and the standard harmonic interaction according to (5) mentioned above.
Case 2 Similar to Case 3 but with weaker bending rod-like extending interaction with $k_b = 10$ and $\phi_0 = 0$ (at zero temperature) with standard harmonic interaction
Case 3 Stiff rod-like extending interaction with $k_b = 120$ and $\phi_0 = 0$ (at zero temperature) with standard harmonic interaction
Case 4 Collapsing structure (at zero temperature) with $k_b = 5$ and $\phi_0 = \pi$ with standard harmonic interaction

The different cases explore the behavior patterns over a wide interaction range; Case 4 corresponds to the situation of a directed bond with intermolecular forces keeping the polyanion collapsed in a confined space whereas Cases 2 and 3 refer to a rod-like topology at zero temperature. Case 1 is a fully flexible chain and Case 4 represents the situation of forces within the polyanion such as when directed bonds are present.

3 Results and discussion

The computations involved

(A) probing the equilibrium structure of the system at different temperatures in terms of :

1. distance correlation functions within the polyanion (Fig. 1), and development of persistence length theories [2]

2. radii of gyration (Fig. 2) and rms end-to-end distance of the polyanion (Fig. 3)
3. radial distribution functions (rdf's) of 1–1 and 1–2 interactions (Figs. 6, 7) for Cases 1–4
4. visual snapshots at 3 temperatures corresponding to the minimum size, maximum size and size at high temperature $T = 10.0$ for Cases 1–4 (Fig. 10)
5. Shape topologies and postulate of ionic bridging mechanism

(B) examining thermodynamics in terms of

1. total energy (Fig. 4) and electrostatic energy at different temperatures (Fig. 5)
2. comparison to the situation with electrostatics turned off (Table 1).

Each of these will be discussed in turn.

3.1 Distance correlation functions within the polyanion and development of persistence length theories

Define the Euclidean distance between atom P_i and P_j of polyanion chain as $d(i, j)$. Then the distance correlation function $D_c(i)$ for interparticle label difference i for a chain length of $N_c = 150$ was defined as

$$D_c(i) = \left\langle \sum_{j=1}^{N_c - i} \frac{d(j, j+i)}{N_c - i} \right\rangle \tag{12}$$

where $0 < i < N_c - 1$. The normal analysis of distance conformation relate to "persistence length" where the Debye-Huckel potential is usually used [41], and where it is acknowledged that the theory is still obscure and not well developed [41]. It is not clear how the normal definitions are directly equatable with the above. The general appearance is that the gradients tend to unity for low and high values, with variable gradient ≤ 1 at intermediate values of i, implying a type of "blob" structure tendency at these intermediate values. The results for Case 1 is given in Fig. 1 only in terms of a logarithmic plot. The plot seems to be consistent with the visual snapshots of Fig. 10 and the graphs of R_g and R_e. The largest gradient is for the most extended regime close to $T = 1.0$. Here the chain is nearly *straight* , according to the snapshots and the high R_g and R_e values and this explains the high linearity of the correlation function , especially at lower i indices; the slight curvature at very high i is due to the kinks and semi-sinusoidal variations of the entire structure which can only be "observed" not locally at low separation distances, but at "global" distances which becomes obvious only at large i because these kinks lower the distance relative to large i, thus lowering the gradient which is not in general the case at lower i values. At high $T = 10$, the same argument applies as the structure becomes more reduced, with more kinks present at shorter separations i, and so not only the gradient goes down, but also the non-linearity of the graph becomes more pronounced. The low temperature $T = .1$ graph is very interesting; at very $low\, i$, its graph is linear and coincides with the other two (implying the same short range structure) but at higher i, the gradient rapidly falls to zero; the nonzero gradient region follows the same argument for nonlinearity as above, but the

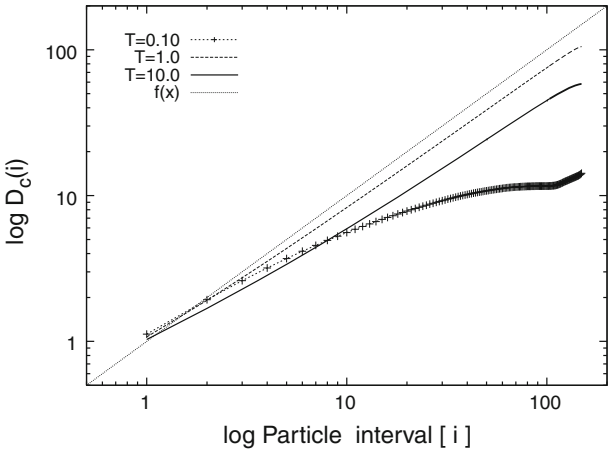

Fig. 1 Distance correlation functions $D_c(i)$ for polyelectrolyte for Case 1, with $f(x) = x$ reference line

snapshots show that the polyanion has curled into a ball shaped structure which can account for the flat gradient if other inferences are made; first if the ball were in fact a type of coil structure with a repeat in the same direction, then one would expect a periodic variation in D_c with i, which is not observed and so it is inferred that the folding is random and inter-penetrating. This seems to be the case according to Fig. 10. The log plot of Fig. 1 reveals another interesting structure if one postulates that $D_c(p)$ has the form $D_c(p) = A(p, T)p^{\delta(T)}$. The plot suggests $\delta(T) \to \backsim 1$ for $T > 1$ and large enough p but where $A(p, T = 1) \neq A(p, T = 10)$. However, at low $T(\backsim 0.1)$ this scaling rule seems inappropriate for at least δ The broad inference here is that the folding patterns can be elucidated from such correlation metrics.

3.2 Radii of gyration and end-to-end distance

The radius of gyration R_g is defined as $R_g^2 = \frac{\sum_{i=1}^{N_c}(\mathbf{r_i}-\mathbf{r_{CM}})^2}{N_c}$ and the average end-to-end distance by $R_e^2 = \left\langle(\mathbf{r_{N_c}} - \mathbf{r_1})^2\right\rangle$ where in the graphs , R_g is actually the averaged value $\langle R_g\rangle$ of the instantaneously defined radius of gyration. Of interest is that the maximum value of both R_g and R_e with respect to temperature variation follows a trend with increasing stiffness as measured by decrease of ϕ_0 and k_b, i.e. for the sequence Case $(4 \to 1 \to 2 \to 3)$, the maximum shifts from right to left in temperature (i.e. from higher to lower temperature), and upwards to higher R_g and R_e values. It is also noticed that the R_g and R_e graphs are similar in shape. According to standard theories and assumptions concerning a long-enough chain length, for polymers that are free to arrange themselves along a persistence length l_p, there exists the relationship $R_e^2 = 6R_g^2$ and the maximum for Case 1 for which there is no angular orientational preference shows a discrepancy of about 30 % about the predicted value; the reason may well be due to the chain being too short for the theory to obtain. One fruitful area then is to create scaling theories of intermediate lengths which can relate R_e and R_g more accurately. The profiles for these quantities Figs. 2 and 3 also show a

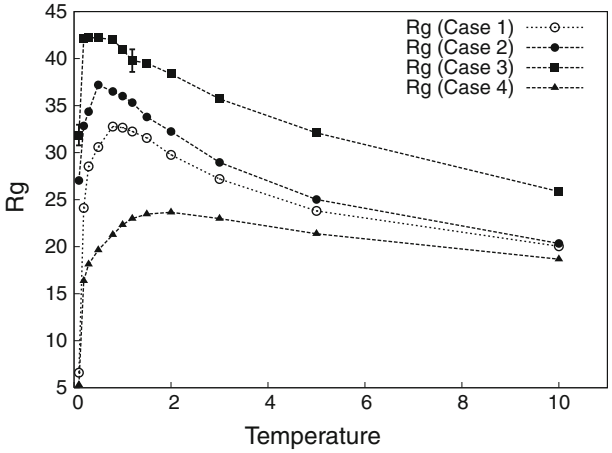

Fig. 2 Radius of gyration for polyelectrolyte

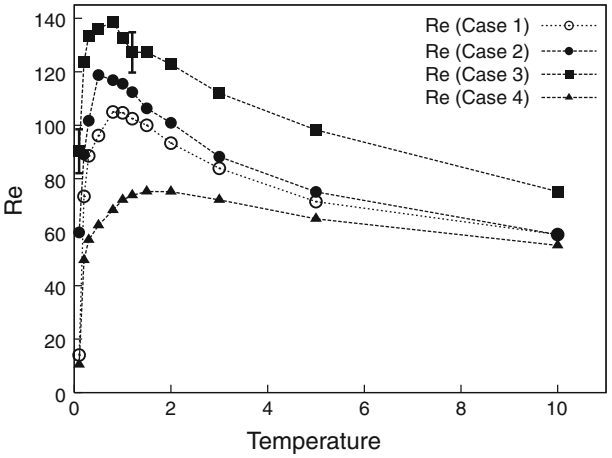

Fig. 3 End-to-end distances for polyelectrolyte

steeper change of gradient from $T = .1$ to the higher temperature maximum along the above sequence. These curves appear typical if compared to those given in [29, Fig. 9] for a chain on a cubic lattice. In conjunction with the energy profile, a phase transition may be indicated according to some interpretations; [1] discusses this point in greater detail. It was found that for Case 3, the very stiff rod-like system implied that the maximum was rather extended with relatively high fluctuations about these points during the equilibrium simulation and the shape at the maximum does not have the pronounced maximum as observed in the Monte-Carlo simulation on a lattice [29, Fig.9] for a simple polyelectrolyte chain.

Some aspects of dipole-dipole induced condensation has been described in [4], where the assumption is that the PE starts to condense the mobile (monovalent) counterions at $e > e_0$, where the PE linear charge density exceeds e_0/l_B, where e, the

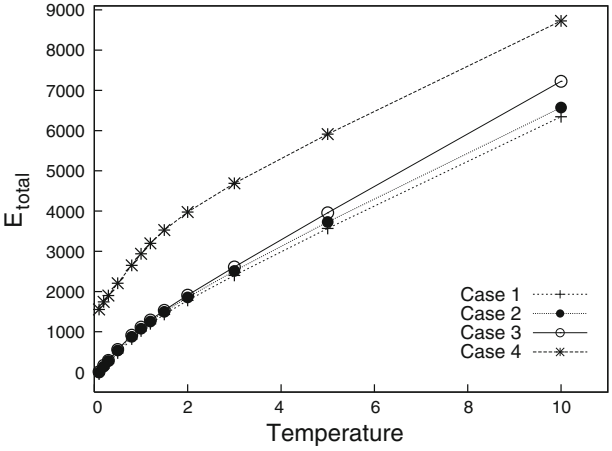

Fig. 4 Total energy for polyelectrolyte

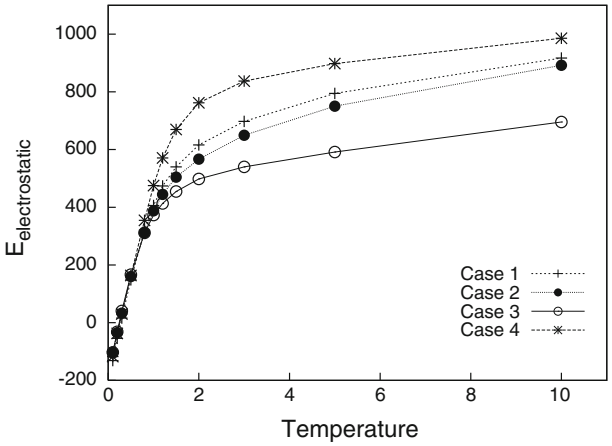

Fig. 5 Electrostatic energy for polyelectrolyte

monomer point-like charge density varies; e is standardized with respect to the Manning prediction for a thin straight PE where θ, the fraction of cations condensed is $\theta = 1 - 1/\xi$, and above the Manning threshold $e(1-\theta) = e_0$. Hence the study seems to presuppose the regime specified by Manning theory, which [1] has shown cannot fully account for the experimental values. It follows that other physical parameters and presumably force-fields stronger than the DH or other PB equation variants might account for the cause, so that what is being described could well represent the forces that prevail after the condensation phenomena. The mechanism for the chain collapse given is D–D interaction (3) of the dipoles perpendicular to the chain length due to the condensed counter ions. The bending or torsional parameters contributing to the forces that would impede the collapse are not described in detail. However, Cherstvy [4] does caution that the Manning prediction is modified by various other factors [4,

his refs. 28,29,53] (which corresponds to [18–20] here). Reference [1] discusses the inadequacy of using DH-type forces to predict or discuss collapse. Figure 3 shows the collapse profile where for a particular electrostatic charge intensity strength (as represented by the temperature T), R_e is dependent on the nature of the twist or bending intensity, whereas the Cherstvy solutions as depicted in Figs. (2–5) [4] for various e/e_0 values and chain lengths does not explicitly incorporated these torsional constants, making it difficult to correlate data in [4] with the results here. One allied topic to the discussion of R_g, R_e and D_c here is the persistence length. We note that the equations used assume continuity, at least of some order of the derivatives; the experimental topologies, on the other hand (e.g. in Fig. 10g) shows well defined kinks that cannot be explained by *local* equations with continuous variables and derivatives. It seems that the thermodynamical equations must also take into account global parameters as well. Such routine incorporation is still at the initial stages, judging from the literature here and in general. One definition of persistence length L_p is given by

$$\langle \cos\theta(s) \rangle = e^{-s/L_p} \tag{13}$$

where s is the distance from the arbitrary point on the flexible polyelectrolyte and $\theta(s')$ is the angle made by the tangent vectors at $s = 0$ and $s = s'$. Obviously this expression presumes a continuous, self-similar behavior where $\theta(s')$ is small; in particular it is not applicable for chains with well-defined kinks (Fig. 10g); nor can this equation apply to chains of indefinite length in a self-similar manner due to the singularities for chains of indefinite length and also for some other reasons that follow. For $s \ll L_p$, we have

$$\left\langle \theta^2(s) \right\rangle \approx 2s/L_p. \tag{14}$$

Using the bending modulus B parameter, the energy of bending can be related to k_b, the harmonic bending potential so that

$$L_p = \frac{B}{k_B T} \tag{15}$$

if one utilizes the Grosberg and Kholkov factor of 2 averaging [42, p. 8] because of 'two independent planes' which seems to provide for the degeneracies in the third dimension although the theoretical justification is probably more involved and not so obvious. Their equation reads

$$\left\langle \theta^2(s) \right\rangle = \frac{2\int_0^\pi e^{-\frac{B\theta^2/2s}{k_B T}} \theta^2(s) d\theta}{\int_0^\pi e^{-\frac{B\theta^2/2s}{k_B T}} d\theta} = 2sk_B T/B \tag{16}$$

which leads to (14). We can relate the bending constant to the B modulus as $\frac{B}{2s}\theta^2 = k_\theta \theta^2/2$ leading to

$$k_\theta = B/b = L_p k_B T/b. \tag{17}$$

For what follows we refer to the development found in [2]. To incorporate the electrostatics (OFS theory), Odijk [43], Skolnick and Fixman [44,45] defined the electrostatic energy change as the energy difference of a straight chained polymer and that with curvature due to the charges on the polymer only neglecting the counterion contribution, leading to

$$\Delta U_{el}(\theta) \sim l_B q^2 \sum_{n=1}^{\infty} \left(\frac{e^{-\kappa r(n)}}{r(n)} - \frac{e^{-\kappa b(n)}}{bn} \right) \sim \frac{l_B q^2 \theta^2}{8\kappa^2 b^3}. \tag{18}$$

Assuming this energy term can be incorporated into k_θ $(= k_b)$ for the total bending energy, they derive

$$L_p = L_p^0 + L_{OSF} = \frac{B + B_{OSF}}{b_B T} \approx \left(B + \frac{l_B q^2}{4\kappa^2 b} \right) / (k_B T) \tag{19}$$

where

$$L_{OSF} = \frac{l_B q^2}{4\kappa^2 b^2 k_B T} \text{ (where } \kappa = 1/r_D). \tag{20}$$

We note that (18) involves summation $n \to \infty$, or $s \to \infty$ which does not fulfill the initial assumptions requiring finite terms. Experiment on the other hand showed a quadratic dependence on r_D as in (20) only at low salt concentration (for large r_D) and a linear dependence at small r_D. Dobrynin modified the OSF theory by incorporating [45] torsional terms in the chain deformation energy energy leading to

$$L_p = L_p^0 + L_{WLC} = \left(B + \frac{0.32 l_B q^2}{\kappa b} \right) / (k_B T). \tag{21}$$

The Manning theory [46] has no linear additive term to Lp; his method is comparative, relating L_p to the persistence length of a null polymer L_p^* where the polymer anionic group is not ionized and it reads

$$L_p = (\pi/2)^{2/3} R^{4/3} (L_p^*)^{2/3} Z^{-2} l_B^{-1} \left[(2Z\xi - 1) \frac{\kappa b e^{-\kappa b}}{1 - e^{-\kappa b}} - 1 - \ln(1 - e^{-\kappa b}) \right] \tag{22}$$

where b is the bond distance, R the radius of the polymer, $\xi = l_B/b$ the charge strength intensity, Z the counterion charge and $1/\kappa_D = r_D$ the Debye screening factor. The above formulation does not fully comply with one or more of the following conditions:

(A.) Equation (16) which relates L_p to B the bending modulus (17) implies inappropriate application of (16) can result in unrealistic values of persistence length
(B.) The energy difference ΔE in the Boltzmann factor is for the total energy difference, where the ES energy must be explicitly included
(C.) $\langle \theta^2(s) \rangle$ is the quantity for a continuous segment and its reduction to bonds is an approximation

(D.) Equation (16) can only be applicable if $s \ll \frac{B}{k_B T}$

The OSF theory derived from (16) has a single summation and so apparently double counts the electrostatic interactions and assumes that the total energy is a linear summation of all the bond energies which does not accord with (B.) above. The Dobrynin (D) theory makes much of the same assumptions are the OSF theory, but one could use the torsional concept by constructing some form of degeneracy about the continuous line segment s. The Manning theory is quite different from the OSF and D theories but in his method [46, p. 3613], it is stated that "the persistence length of DNA is many more times larger than the persistence length of its uncharged isomer" but from calculations [2, p. 52, Fig 3.19] at salt concentrations $>$ 50M, his L_p is negative. These observations seem to imply that the DNA L_p cannot be smaller than the corresponding uncharged DNA for at least some concentration regimes, which contradicts simulation experiments (see results in [2, p. 46, Fig. 3.15(a–d)]. In attempting to derive a preliminary alternative and first order expression for L_p that satisfies the conditions (A-D.) above, Agung [2, p. 28] writes the energy expression over a finite number of terms to satisfy condition (D.) of a chain of n bonds arranged in a circular arc ($s = nb$) where

$$\Delta E = \frac{B\theta^2}{2s} + \sum_{i=1}^{n} \sum_{j=i+1}^{n+1} \frac{l_B k_B T q_i q_j \exp(-\kappa r_{ij})}{r_{ij}} \tag{23}$$

with $r_{ij} = nbG$ and

$$G(n, \theta, i, j) = \frac{1}{\theta}\sqrt{2(1 - \cos[(\theta/n)(j - i)])}. \tag{24}$$

We use the Grosberg averaging method to compute $\langle\theta^2\rangle$. We realize that there are other averaging methods to take into account the third dimension that can be developed or utilized in the future. The Dobrynin use of torsion is one example of introducing effects due to the third dimension. From the computation of $\langle\theta^2\rangle$, we derive $L_p^0 = \frac{B}{k_B T}$ (due to normal bending and torsional motion in three dimensions) and the electrostatic contribution to the persistence length becomes

$$L_p^{el} = \frac{2 l_B q^2 n}{\theta^2} \sum_{i=1}^{n} \frac{(n - i + 1)}{i} e^{-\kappa b i}. \tag{25}$$

By observing the exact form of (25) by using a computer symbolic algebra simplification where some separation of variables was possible, a curve fitting to the form [2, p. 34, eq. 3.35] was attempted:

$$L_p^{el} \sim 2 l_B q^2 n < \langle f_1(n)\rangle_b e^{-\kappa b \langle f_2(n)\rangle_b} >_\theta . \tag{26}$$

The form for determining functions f_1 and f_2 was derived by fitting with simulation data over a wide concentration range. The final form from the extensive curve fitting for L_p in Å units is:

$$L_p = L_p^0 + 2l_B q^2 n(0.0071n + 0.0234)(b/l_0 + 21.17)^{-0.052\kappa bn} \tag{27}$$

where $l_0 = 1$Å for dimensional consistency. We note that (27) is n or segment dependent, The above expressions of Agung (A) , OSF, Manning (M) and D are compared to simulation experiments ([2, Fig. 3.15 a–d])for the standard DNA monomer of radius 10Å with NaCl counterions of radius 2Å, where the salt concentration c_s varied from 0 to 0.25mM, and for this regime, the persistence length $L_p = 1100$ at $c_s = 0$ to ~ 400 for $c_s = 0.25$mM where $L_p^0 = 500$Å, which implies that $L_p^{el} < 0$, which cannot be accounted for for all the theories above (M, OSF, D and A). Further, the A theory passes very approximately midway through the graph at ~ 900Å , passing through some of the experimental points whereas OSF, D and Manning are significantly off-scale. At very high c_s concentrations ($\sim 1.0 - 900$mM) where computer simulation data were not available due to limits of computer resources, data from real experiments which have large experimental scatter show that within error uncertainty the A,M and D models approach experimental results, but the OSF theoretical values are off-scale except for very high concentrations ($\sim 200 - 900$mM)[2, Fig. 3.18, p. 50]. The real experimental data were derived from Smith et al. [47], Nordmeier [48], Baumann et al. [49] and Rizzo et al. [50]. Agung [2, p. 51] proposes that the inequality $L_p^{polyelectrolyte} < L_p^{neutral\ polymer}$, a condition impossible for at least the OSF and D theories can be accommodated into A theory by postulating an "ionic bridging" mechanism, where the ff's due to highly symmetrical solutions of the PB equations are not applicable, and where as a result of the mobile cation accumulation, the DNA polymer is bent or curved in one particular orientation which is borne out in detailed simulation snapshots (e.g. Fig. 3.21, p. 55, Fig. 3.22, p. 57). Two modifications are therefore proposed to A theory that might account for the anomaly:

1) Replacement of the D-H ff's by another asymmetrical one
2) Introduction of a degeneracy factor $G(\theta)$ into the Grosberg averaging process [2, p. 56] where

$$\left\langle \theta^2(s) \right\rangle = \frac{2\int G(\theta)\theta^2 P(\theta)d\theta}{\int G(\theta)P(\theta)d\theta}. \tag{28}$$

If this "ionic bridging" exists (giving rise to the asymmetrical curvature of the polyanion) the $G(\theta)$ would increase $\left\langle \theta^2(s) \right\rangle$ and therefore decrease L_p.

With the above discussion of persistence length, R_e and $D_c(i)$ can be viewed not only as indicators of topology, but as bearing some relationship to L_p under certain assumptions. Assume that the coordinates of the last monomer of the polyion is at $\mathbf{r_n}$ ($\mathbf{R_e} = \mathbf{r_n} - \mathbf{r_0}$) and that n is small enough for (14) to be used for L_p determination. Defining $\mu_\mathbf{i} (= \mu_\mathbf{1}) = \mathbf{r_1} - \mathbf{r_0}$ as the bond vector where $b = | < \mathbf{r_1} - \mathbf{r_0}| >$ is the average bond length, then the previous equations lead to

$$\ln \left\langle \frac{\mu_\mathbf{i}.\mathbf{R_e}}{R_e b} \right\rangle = -nb/L_p. \tag{29}$$

Assuming a sufficiently low correlation between any instantaneous $R_e = |\mathbf{R_e}|$ and $\mu_\mathbf{i}.\mathbf{R_e}$ then (29) can be written

$$\ln\langle R_e\rangle \approx \ln\langle \mu_\mathbf{i}.\mathbf{R_e}\rangle + \frac{nb^2}{L_p} \tag{30}$$

where $nb = s$ is the contour length. If $\ln\langle \mu_\mathbf{i}.\mathbf{R_e}\rangle$ is fairly constant (one can expect that although R_e increases with n, the angle θ on average will also increase, nullifying the increase in the scalar product), then $\ln\langle R_e\rangle$ is approximately linear with n as suggested in [4, Fig.2–3]. If L_p is deemed constant, then $\langle \mu_\mathbf{i}.\mathbf{R_e}\rangle$ may be determined as a function of n, if $< R_e >$ is known from experiment. With simulations, all the above equations can be tested. Similarly for (30), under the same assumptions, with $\mu_{\mathbf{i},\mathbf{0}}$ representing the initial bond vector, one might write

$$\ln(|\mathbf{D}(i)|) \approx \ln\langle \mu_{\mathbf{i},\mathbf{0}}.\mathbf{D}(i)\rangle + \frac{b^2 i}{L_p} \tag{31}$$

For Case 1 (Fig. 1) with no bending mode, a fairly linear profile is observed at higher T implying a near unity and/or constant value of $\langle \mu_{\mathbf{i},\mathbf{0}}.\mathbf{D}(i)\rangle$. The departure at low $T = 0.10 \Rightarrow \langle \mu_{\mathbf{i},\mathbf{0}}.\mathbf{D}(i)\rangle \ll 1$ or some type of constant orientation of the tangent vector of the polymer chain w.r.t. the s distance. Figure 3 gives some information of the $\xi = 1/T$ charge intensity parameter and how this influences the $\mu_\mathbf{i}.\mathbf{R_e}$ factor. With an apparent convergence at high T, if $\ln|\mu_\mathbf{i}.\mathbf{R_e}| \to 0$, then a high temperature limit to L_p may be computed. The relationship of R_g to R_e and the above equations is less clear-cut. Cherstvy (C) [4, his ref 23] provides data extracted from literature in Fig. 5 where the R_e^2 scales as $R_e^2 \sim e^{-2}$ [4, Eqn. 15] where as before e is the net or apparent monomer charge and at high chain charge density e/e^0, R_g^2 also scales as for R_e^2 ($\sim e^{-2}$) [4, Fig. 5]. C also discusses other contributions, where the size is said to scale as $R \propto N^{1/3}\xi^{-2/3}$, where N is the chain monomer number and ξ the Manning-like parameter. It seems that the data in Figs. 1, 2 and 3 would require perhaps further development of current theories to account for the results quantitatively at each point in the curve even though the scaling behavior as reviewed here might be adequate.

3.3 Energetics

At low temperatures, one observes a convergence in electrostatic energy for all the Cases (1–4) in Fig. 5, including Case 4. On the other hand, where the total energy is concerned, there is a curious separation of Case 4 from all the others which refer to either stiff external bonds or no bending interactions. In Case 4, the collapsed bonds are stretched out at higher temperatures, which can be inferred from the snapshots of Fig. 10; therefore in this complex situation, since the bending modes are still quadratic in nature, there is an interesting coupling of this to the non-bonding LJ and Coulombic interactions that allows for a much higher energy state that what strict equipartition taken in isolation would allow. The interaction and collisions with the free cations seem to extend the bond angle by some coupling mechanism so that the system can

be viewed as one potentially of energy storage; as $T \rightarrow 0$ then also $E_{tot} \rightarrow 0$ and the curves for Case (1–3) all coincide except for Case 4, where the snapshots show a ball-like configuration at low temperature but a relatively high energy due probably to the repulsions of the anionic particles not neutralized by the counterions, unlike the others. As the brief survey of size and shape functions (e.g. R_e, R_g, $D_c(i)$) indicates, the theoretical descriptions are on-going, often with the introduction of higher-order approximations within the same overall theoretical structure. It seems that the thermodynamical descriptions might also follow such trends. Polyions and DNA strands have been modeled at the simplest level by using the Poisson–Boltzmann Cylindrical Cell Model (PBCCM) [2,7–9] where the polyion is an infinitely long charged rod with charge spacing (bond length) b placed in the center of a cylindrically symmetrical sheath of radius R_c from the polyion central strand and with a surface parallel to the strand axis [2, Fig. 4.4]. Defining $\xi = l_0/b$ as the electric charge intensity parameter (where l_0 is the Bjerrum length and b the distance between charges or the bond length, the PBCCM potential solution has been derived such that the electrostatic contribution to the energy E_{el} and entropy S_{el} per polyionic charge surrounded by salt and counter-ion has the form [7–9]

$$E_{el}/[k_B T] = \frac{\xi}{2l_B}\phi_m + \int_{r_M}^{R_c} 2\pi r \sum_{\alpha}(z_\alpha \rho_\alpha(r))\phi(r)dr \tag{32}$$

for the energy, and the entropy [7,9] is given by

$$S_{el}/[k_B T] = -\int_{r_M}^{R_c} 2\pi r \sum_{\alpha} \rho_\alpha(r) \ln\left[\frac{\rho_\alpha(r)}{\rho_\alpha^0}\right] dr \tag{33}$$

where r_M is the distance from the center of the polyion to the surface. R_c is determined via the DNA concentration term $c_{DNA} = \frac{\xi}{4\pi l_B N_A R_c^2}$. Both Eqs. (32–33) as written down explicitly are dimensionally inconsistent (they have dimension of L^{-1} on the *rhs*). Korolev [7] and Stigler [9] computed ϕ_M and $\phi(r)$ using PBCCM and the RDF function as the concentration ratio

$$g(r) = \frac{c_{i,M}}{c_{i,\infty}} = \exp\left(-\frac{z_i e \psi(R_{i,M})}{k_B T}\right) \tag{34}$$

where $R_{i,M}$ is the distance of a mobile ion to the polyion surface. These choices when solved do not reproduce the typical $g(r)$ structure derived from simulations or experiments with the typical fluctuation of mobile cations with the distance from the polyion [2, Fig 4.5, p. 69 shows comparison with simulation] due to the uneven distribution of charge along the polyion. Furthermore, κ, the DH screening parameter ignore the 'third' particle-type, meaning that the polyions are not accounted for in the determination of κ (via the ionic strength term in the DH theory) which implies that the potential and particle density obtain only for regions that are perpendicular to the

axis of the DNA rod about a vertical distance b with no lateral interaction with the potential differences along the polyion axis. To introduce this effect, the influence of the other polyions, and to make the equations dimensionally self-consistent, Agung [2, Sect. 4.4.1, p. 68] transformed the parameter l_B/b to l_B/Nb to denote the unit over the polyelectrolyte length and introduced the density of mobile species α as $\rho_\alpha(r) = \rho^0_\alpha g^i_\alpha(r)$ where $g^i_\alpha(r)$ is the RDF of the α-type particle due to the monomer i on the polyion summed over a convenient interval N (which may be the total number of monomers), and $g_\alpha(r) = \sum_{i=1}^{N} g^i_\alpha(r)/N$. Then (32) takes the final form for the energy

$$E_{el}/[k_BT]/(\text{unit length}) = \left[\frac{N}{2}\phi_m + \frac{N^2 b}{2}\int_{r_M}^{R_c} 2\pi r\Big(\sum_\alpha z_\alpha \rho^0_\alpha(r) g_\alpha(r)\Big)\phi(r)dr\right]/Nb \tag{35}$$

and the entropy [7,9] is given by gross simplification of uniform or similar g function over a very long chain as

$$S_{el}/[k_BT]/(\text{unit length}) = \left[-\int_{r_M}^{R_c} 2\pi r N^2 b \sum_\alpha (\rho^0_\alpha(r) g_\alpha(r) \ln g_\alpha(r))dr\right]/Nb \tag{36}$$

where more general expressions are also developed [2, eqs. 4.21–4.23]. The $\phi(r)$ potential is solved by using the PB equation for a cylindrical cell [9]. The above is a study in its own right but these equations were successfully used to determine E_{el}, S_{el}, and F_{el} (Helmholtz Free Energy) for a spherical distribution of mobile counterions about the polyion for the DNA-NCP interaction by a transformation of coordinates [2, p. 76, Figs. 4.6(a–b)]. The F_{el} minima occurs about a flat plateau about the salt concentration [0.001–0.01]mM that compares favorably to the simulation snapshots of a system with 12 NCP particles interacting with the 360 unit long DNA strand [2, p. 79, Fig 4.9] where maximum number of binding of the NCP particles to the polyion is observed in this regime of salt concentration. There is also some correspondence with the data from [12].

3.4 Distribution functions

The RDF's were checked using the well known expression

$$\rho_j \int_0^R 4\pi r^2 g_{i\,j}(r)dr = n_j \tag{37}$$

and was found to be accurate to at least .1 % and furthermore the RDF's were normalized in the standard manner as with $g_{i\,j}$ in (37) where ρ_j represents the average bulk

density and n_j the absolute number within the sphere of radius R ; The apparently high values of the RDF's are due in part to the box volume of 8×10^6 units and the fact that a single chain with bounded beads were featured in the system; $\log_{10}$ scales were used in the plots. The treatment of complex systems would require the development of RDF's that are orientation dependent; despite some peripheral hints scattered in the literature, no exact theory has been developed. This also results in computer packages implementing algorithms that pertain to isotropic radial pair distributions. Thus at this stage of the development, the thermodynamics cannot be numerically computed from these distributions accurately, and these distributions must be interpreted with the snapshots such as provided in Fig. 10. Figure 6a, b depicts Case 1 for the 1–1 (a) and 1–2 (b) interactions; the 2–2 free cationic interactions are uniformly spread out and are not too relevant here. In the graphs, the rdf's all tail away in a near exponential manner and attention is paid to the interactions (to about 4 unit distance) close to the polyanion vicinity. The rdf seems consistent with the visual structure in Fig. 10. The low temperature ball like structure with random winding (as discussed above Sect. 3.1 implies at low distances a rather flat distribution with the maximum shifted to the right because the low kinetic energies do not lead to closer proximity to the negatively charged atoms on the polyanion; the extended structure, which is very labile but nevertheless relatively "straight-chained" and therefore has a regularity that is displayed in the zig–zag periodicity observed at $T = 0.8$ with maxima (minima) separated by distance $\sigma = 1$ the diameter of the LJ interactions. The high temperature $T = 10$ structure is mid-way between these other two, and because of the higher kinetic energy, leads to the maxima located to the left of the others. The argument for the maxima or first zero point for the 1–2 interactions in Fig. 6b is analogous to the 1–1 interaction; high temperatures allow for a greater spatial exploration of particles 2, leading to an almost zero gradient at high internuclear distances; and the heights of the rdf's vary in opposite manner to the temperature; the lower kinetic energies of particle 2 implies that they would congregate closer to the negative core and further, they would be less likely to be found at further distances implying some type of power-law decay in the amplitude of he curve; this is observed for the curves at $T = 0.8$ and $T = 0.1$. Another interesting observation is a hint of periodicity for the $T = .1$ curve; particle 2 is non-bonded, but its finite size arranged about the globule leads to this partial periodicity in the same sense of typical liquid phase RDF's.

Case 2 Fig. 7 is very interesting especially when interpreted in relation to the snapshots in Fig. 10d–f. Unlike Case 3, the rod-like orientation of the bending mode has a weak bending constant of $k_b = 10.0$. There does not exist any noticeable kinks and so the RDF's would approximate at low temperature those for Case 3 for higher temperatures. At all stages of the 1-1 interactions, semi-periodicity is seen as for a typical string structure, but the much lower bending constant implies that type 1 atoms would interact such that no distinct bands of non-zero value would form; this is what is observed; the semi-periodic structures are seen and become indistinct at high T as the periodic bands merge and overlap. The interpretation for the 1–2 interactions follows as for above, where the open string nature of the polyanion allows for some semi-orderly arrangement of the 2 cations at low temperature; this feature is gradually lost as the temperature increases.

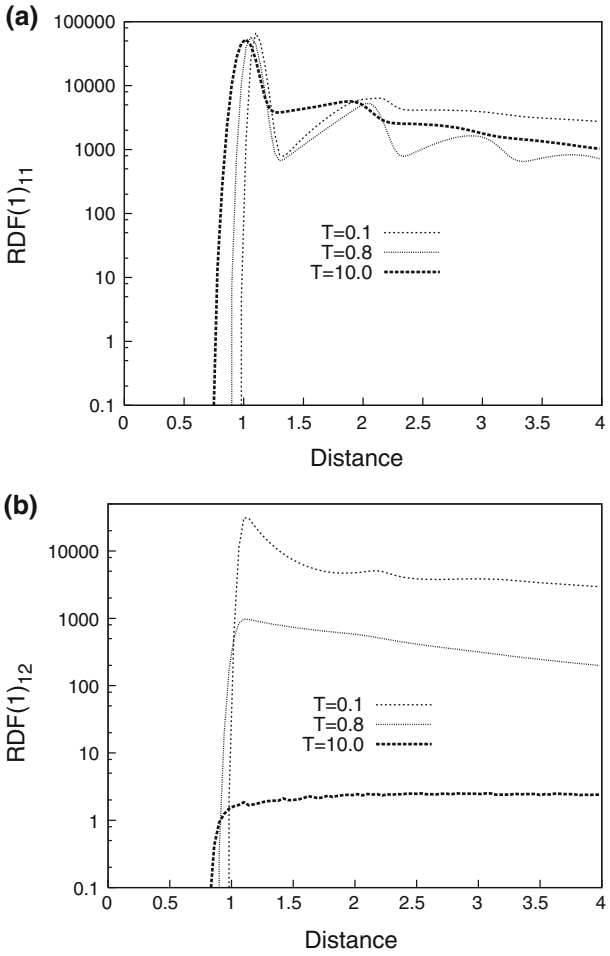

Fig. 6 Case 1 RDF for **a** $1-1$ interactions, **b** $1-2$ interactions

Case 3 (Fig. 8) represents rod-like interaction with a high bending constant; the simulations show large fluctuations as is evident from the error bars of the R_g, R_e figures at low temperatures and at high R_g, R_e of the graph. There is a dramatic change in the form of the RDF, but viewed qualitatively and visually via the snapshots, the structures are linear with a central kink or kinks. It seems that one method to determine whether a phase transition is involved is to examine the mean-squared fluctuations of the energy or other variables that are pertinent rather than to use topological characteristics such as "shape". In any case, Case 3 (Fig. 8a) suggests (for 1–1 interactions) a type of tautomerism of structures that have features of the cold $T = 0.1$ state and those at high temperatures for the region $T = 0.2 - 0.8$ about the region where the maximum R_g is located. The 1–1 interaction at $T = 0.1$ shows not a globular structure but one where there is generally a single kink centrally located in the polyanionic chain (Fig. 10g–i). The two arms of this kink oscillate, so that although there is limited bending motion

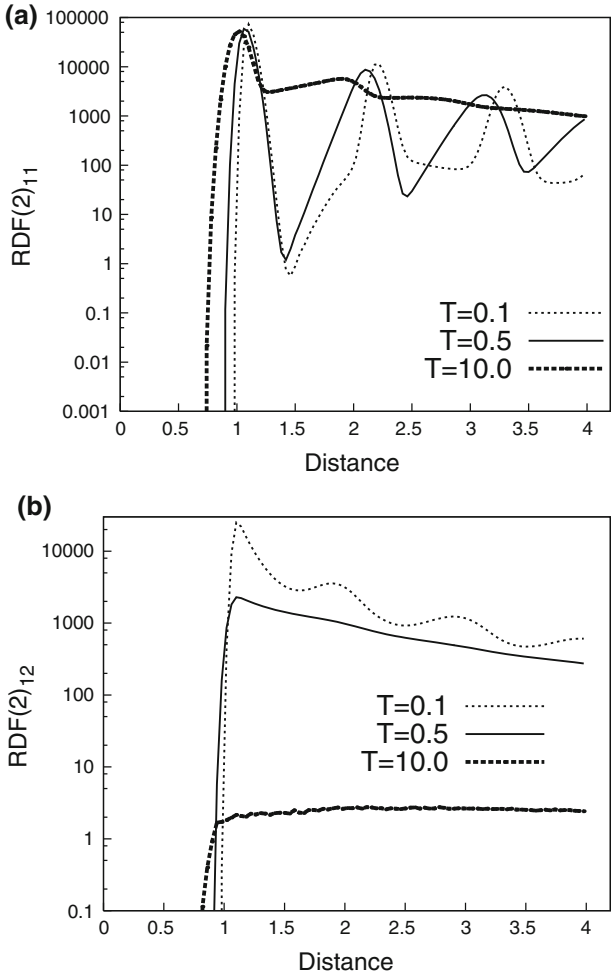

Fig. 7 Case 2 RDF for **a** $1-1$ interactions, **b** $1-2$ interactions

about the monomer bonds (except where the kink is), the proximity of the two arms leads to the breakdown of a periodic lattice structure with distinct maxima and minima ; kinks also appear at the ends of the chain. In the case of $T = .2$, the symmetry of the kink is broken and the kink seems to be transfer more to the end-point atoms of the chain (Fig. 10h). Thus both are periodic structures moderated by the presence of a kink that leads to similar RDF's except for the details between the maxima due to the different positions of the kinks. At slightly higher temperature ($T = 0.5$), the kink structure is not favored and the structure reverts to a curved structure whose R_g value is slightly smaller than that of a straight structure with a kink , at $T = .2$ but whose RDF shows clear periodicity but with a broad band about the region of non-zero value. At much higher temperature, this periodicity is partially retained, but the bending and harmonic vibrations are large enough to span the band so that no non-zero

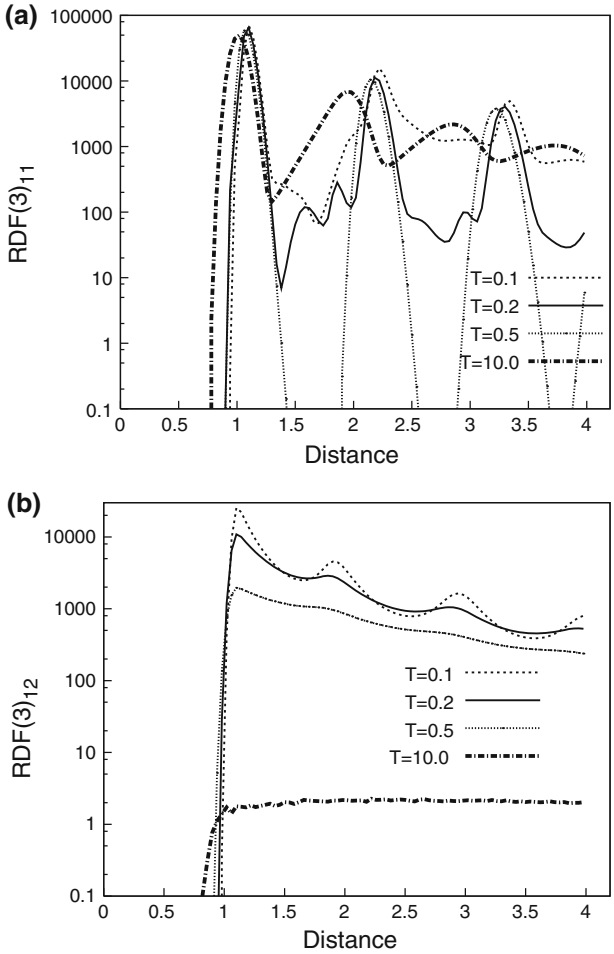

Fig. 8 Case 3 RDF for **a** $1-1$ interactions, **b** $1-2$ interactions

value exists. The 1–2 interaction RDF (Fig. 8b) can be interpreted as for Case 1 above with basically the same features but here at $T = 0.1$ the periodicity is more obvious, probably because the symmetrical kink with bare charge polarizes the cations so that they assume a semi-periodic arrangement about the polyanion; this periodicity is lost at higher temperatures due to the greater irregularity of the polyanionic structure and the kinetic energy of the free cation counterions.

Case 4 RDF 1–1 interactions Fig. 9 follows that same arguments as for Case 1, the random coiling destroys periodicity except for the first and second neighbor distance because of the presence of a collapsing bending mode that draw nearest neighbors together. At higher temperatures, for the 1–1 interactions this periodicity is lost because of the coiling motion due to the low value of $k_b = 5$ as the snapshots depict Fig. 10j–l. The 1–2 interactions follows the same arguments as above; the features are all quite similar; only the intensity of the periodicity at low temperatures differ.

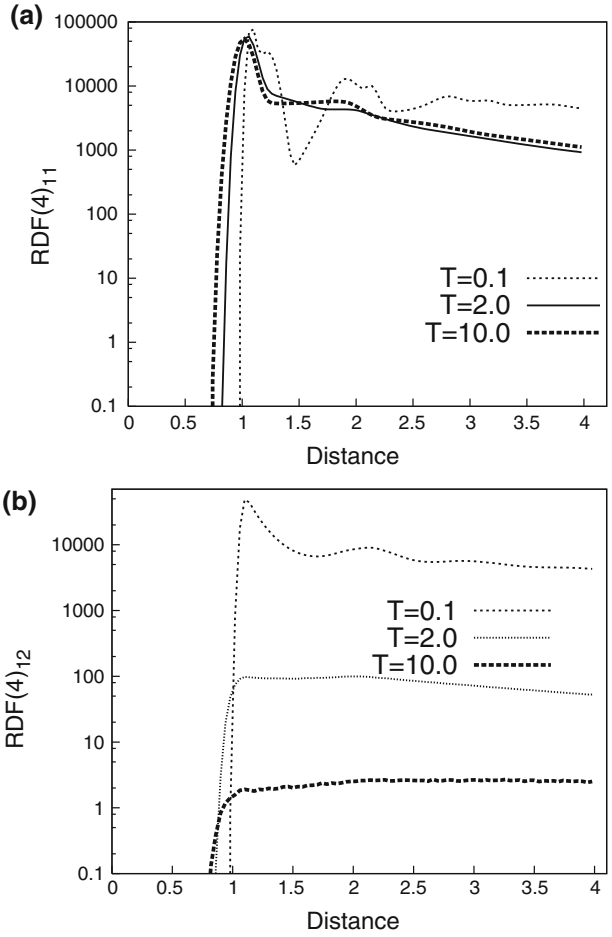

Fig. 9 Case 4 RDF for **a** $1-1$ interactions, **b** $1-2$ interactions

General remarks: The 1–2 interactions show a reasonable exponential drop in the RDF with distance since the log-distance plots are linear. One might write the observation as $RDF = A \exp -k(T)r$ where $k(T) \to 0$ as $T \to \infty$. The gradient characteristics are less evident for the 1–1 interactions which are localized, but here, the gradient of the plots for the different temperatures seem to be quite similar. At present no comprehensive theory exists for non-isotropic species distribution that can predict or categorize phenomena such as phase transitions. For instance, from the visual examination of the snapshots, we note that the shape of the RDF's cannot in all cases be unambiguously assigned to the respective snapshot. We note that theories of phase transitions are based on simplistic model systems with well defined boundary conditions that do not obtain for soft-matter complex systems. Thus in the absence of robust theories for complex systems involving many species types and interactions, the debate concerning whether phase transitions occur or not in this system [1, Sect.

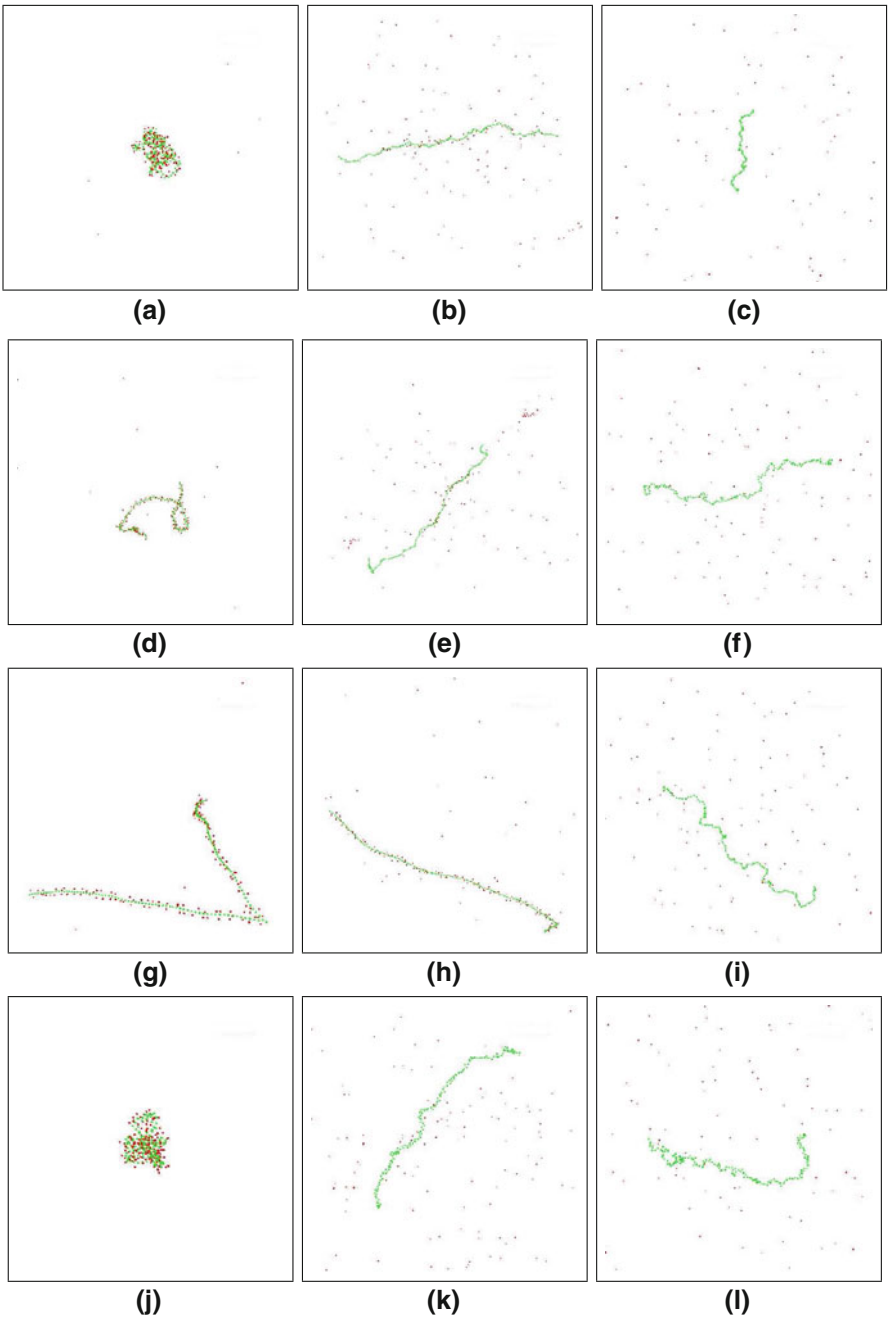

Fig. 10 Snapshots for Cases 1–4: Case 1 **a** $T = 0.1$, **b** $T = 0.8$ and **c** $T = 10.0$; Case 2 **d** $T = 0.1$, **e** $T = 0.5$ and **f** $T = 10.0$; Case 3 **g** $T = 0.1$, **h** $T = 0.2$ and **i** $T = 10.0$; Case 4 **j** $T = 0.1$, **k** $T = 2.0$ and **l** $T = 10.0$

3.1 and the refs. 5,30, 36, 37 therein] can be held tentative until more data especially concerning the energetics (energy and other thermodynamical fluctuations, connected to say the specific heat) is measured. Perhaps unfortunately, many well established MD software are based on synthetic algorithms [51, Sect. 3.4] where non-Newtonian equations of motion are integrated to maintain the constancy of certain thermodynamical variables; these synthetic algorithms await rigorous proof that demonstrates that the deterministic 'fluctuations' of these continuous systems are equivalent to those of mechanical systems conforming to Newton's laws but subjected to stochastic disturbances so that they may be used to determine fluctuations of purely mechanical systems to yield associated information like the specific heat from the fluctuations. However, one can always resort heuristically as with experimentalists to defining phase transitions in terms of threshold of such variables. In real experiments involving polymeric and ionic liquid molecules, differential scanning calorimetry (DSC), NMR and X-ray scattering has been used to characterize transition phases [52, p. 60, Sect. 3.1.2.1].

3.5 Snapshot commentary

As demonstrated above, visualization can be a valuable tool of interpretation for structural parameters. The snapshots below are not to scale, but have been captured to qualitatively assess the various configurations. Three extreme configurations of polymers have been described by Haug in his triangle [53, p. 358]; here we illustrate how for a single system, all three (and more, as in the symmetrical kink structure) may be realized over a temperature range. Figure 10a (Case 1) shows a globular structure despite same charge repulsions which long-range interactions can induce in a manner which is perhaps not intuitively obvious, this polyanion reaches its maximum size at quite low temperatures (b of same figure) , before again shrinking in size at higher temperature (c of Fig. 10), which is also not intuitively obvious. As with all these cases, it may be surmised that the mean kinetic energy of the particles might be involved in these transformations, and not merely the potentials.

Case 3 for a stiff, rod-like polyanion is depicted in Fig. 10g–i; (a) shows a non-globular symmetrical kink structure at low temperatures, with some further kinks at the ends; (b) shows an elongated straight structure and (c) shows multiple kinks along the entire chain, leading to a reduced R_g.

Case 4 Fig. 10j–l is again counter-intuitive because here, the bending vibrational mode draws the type 1 atoms closer ; (a) shows that at low temperatures a globular structure prevails, and (b) shows the polyanion at its largest at $T = 2.0$ despite the bending mode which would force it to collapse, whereas (c) shows that at high temperatures, even when it can overcome the natural forces of contraction, it then assumes a smaller, more bent size. This example shows that long-range electrostatic forces induces pattern and shape formation that may not be obvious. Case 2 (Fig. 10d–f) is the same as Case 3 except for smaller bending constant $k_b = 10$. Here, there appears at low temperature the same tendency toward contraction by the external ionic atmosphere, whereas this is relieved at intermediate temperatures only to be subjected less drastically to the same external forces that favor contraction at $T = 10.0$.

Table 1 Results for polymer situation with electrostatic interactions turned off for system type A–C

Type	R_g	R_e	E_{total}
A	$9.92 \pm .2$	$24.07 \pm .5$	$604.98 \pm .04$
B	$31.70 \pm .4$	87.0 ± 2.0	$747.5 \pm .2$
C	$8.1 \pm .2$	$20.4 \pm .4$	$34424.60 \pm .2$

3.6 Reference system without electrostatic interactions

The predominant forces in this system are due to electrostatic interactions. As a comparison with a reference, a system which is identical in all respects except that the electrostatic interaction was switched off completely was studied all at the same temperature $T = 1.0$, close to the maximum R_g namely:

Type A Case 1 with the same parameters without electrostatic interactions
Type B Case 3 with the same parameters, without electrostatic interactions
Type C Case 4, with same parameters except $k_b = 120$, without electrostatic interactions

For the above , the non-bonded LJ potentials and the bonded potentials were retained.

Table 1 provides some basic information. Type C was included to illustrate that in a mixed environment where the coordinates were involved not just in bonding modes but also in dispersal interactions, there is a general collapse of conventional quadratic equipartition as witnessed by the very high E_{total} of which the total energy amounts to $(34, 424.60 \pm .2)$ as the structure is not stabilized by electrostatic interactions leading to the opening up of the dihedral angle of the uncharged polymer chain due to interactions with the polymer skeleton primarily and secondarily the "counterions" which could interact if a large scattering cross-section were presented in for instance a blob or other similar structure. This is not the case for the bond energy for types A and B. Also, most of the energy from the polyelectrolyte is from the electrostatic contribution, from both the 1–1 and 2–2 repulsion energies since the other 1–2 interaction is negative in sign and one can compare the total energy of Type A and B with their Case 1 and 3 analogs. The R_g, R_e values for Type A is severely diminished, implying some type of long-range electrostatic energy which can stabilize the system for Case 1 interactions; it may be conjectured that the large negative charge repulsions on the polyanion tend to keep these charges far apart, and that because the positive charges have not condensed about the polyanion boundary, local repulsive forces predominate. The details of the interactions appear not to have been worked out even for this simple model. Type B interactions have large R_g, R_e values due to the large bending constant and the direction of the interaction. In this case, one might conjecture that for Case 3, the large R_g and R_e values are due to both the large k_b value and the electrostatic repulsions which are not screened by the positive counterions; screening is effective at lower temperatures as the counterions condense on the polyelectrolyte skeleton, diminishing the magnitude of electrostatic interactions. Type C interactions show that if the coordinates are mixed and fairly complex, equipartition would not obtain for classical systems implying that the coordinates of a particular system must be examined

to ensure that they are canonical and that they are separable from other coordinates (for the vibrational modes); failure to do so may allow for interpretations that assume canonical distributions when this does not obtain [54] in terms of MD evidence.

We show later that where distribution functions are concerned (such as RDF's) different models with different charge allocations [52, p. 207] on atomic sites can lead to very different outcomes. Although charge allocations in a particular simulation is ambiguous even when advanced quantum calculations are made, treatises often [52] do not provide much data correlating these allocations with simulation outcomes and experimental results. For such inorganic and non-biological organometallic systems, such information may not be considered significant relative to the other forces that predominate. On the other hand, these correlations for biological systems are probably very significant; if found to be so, then another set of finer-grained MD would be initiated as a routine.

4 The effects of the monomer model chosen to the radial distribution function and persistent length

Much has been written and data generated to provide parameters for simulation whose results are then correlated with experiments [52, Sect. 4.2]. Here is discussed the effect of modeling the monomers of the polyanion DNA strand to the counterion distribution profile by reasonably varying the charge distribution of the polyanion in the manner below. We simulate a DNA-salt solution at fix temperature 300 K. From experimental data, DNA is a polyelectrolyte where each phosphate group along the DNA chain has charge -1. The axial distance between two consecutive phosphate groups is 1.7 Å, The diameter of the DNA chain is 20 Å. We apply two kinds of monomer models. In the first model, 6 base pairs of DNA containing 12 phosphate groups are united as one monomer. Thus each monomer has charge -12 and the monomer–monomer distance 20.4 Å. The monomer radius 10 Å is fulfilled by applying appropriate parameters as before for the Lennard-Jones non-bonded potential between monomer and ions. The DNA monomer model has radius 10 Å, constituting 8 Å hard-sphere and 2 Å soft-sphere radius in the LJ-type interactions defined in the Expresso package. The Na^+ and Cl^- ions have 2 Å soft-sphere radius with zero hard-sphere radius. For the second model, the monomer point charge is -1 and the monomer–monomer distance is 1.7 Å. The LJ parameter for the monomer–ions nonbonded interaction for the second model equals that for the first model to define a 10 Å radius chain. The DNA concentration is chosen to be 2.0 mg/ml (within the real life experimental regime) and the salt 1:1 concentration is 10 mM. The total amount of monomer for the first chain model is 60 and for the second model is 720 implying the same contour length and simulation box length possessed by both models.

The RDF between DNA and Na^+ ion for both models is depicted in Fig. 11). First we compare the first peak of the RDF profiles ($r \sim 12.5$ Å). This is related to the Na^+ concentration at the polyelectrolyte surface. The concentration of Na^+ at this distance for the first model (dotted line) is much larger than the second model (solid line). This is reasonable on physical grounds since the monomer charge of the first model is many times larger than the second model. Another difference is that in the first model the

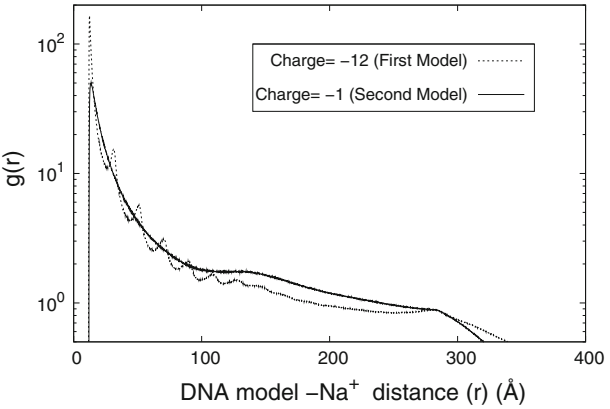

Fig. 11 The DNA–Na^+ RDF from two different DNA monomer models

Na^+ concentration accumulation starts even at a distance smaller than the sum of the DNA-Na^+ radius (12 Å), due to the strong monomer–Na^+ attraction. For example at distance 11.88 Å, the RDF of the first model has value 34.72 and for the second model it is 0.42.

The obvious difference of the shape between the first and second model RDF is the fluctuation or oscillation in the DNA-Na^+ RDF of the first model (dashed line). At equilibrium we find the fluctuation is quasi-periodic with peak distances about 18–21 Å. Since the Na^+ ion radius is 2 Å, it is clear that the rdf oscillation does not occur due to the Na^+ condensation layer. These observations of such oscillations suggests the non-uniform Na^+ condensation at the polyelectrolyte surface. The shorter the distance between a point to the monomer point charge, the bigger the negative potential felt by that point due to the monomer charge. The more negative the potential at any point, the more probable it is for the Na^+ to exist there at that point. Since the monomer bond distances and the bonding and physical parameters of the monomers are set to be the same throughout the polyelectrolyte, the non-uniformity is periodic along the chain axis. Since the distance between two monomer point charges in the first model is relatively large (20.4 Å), the non-uniformity of the Na^+ distribution within a surface perpendicular to the bond axis could be clearly detected. Thus in the first model, the RDF from a central monomer oscillates over a radial distance range because of the non-uniform Na^+ concentration at the surface monomer neighbors.

In the second model, the distance between two consecutive point charge is much smaller than the first model. Also the monomer–monomer distance 1.7 Å is smaller than the Na^+ radius 2 Å. It creates a relatively uniform charged surface for the Na^+ counterion. As a consequence, in the second model we do not observe any distinct oscillations due to the inequality of the amount of the Na^+ ions condensed at the polyelectrolyte surface.

Another point is if we do not consider the peaks due to the Na^+ accumulation at monomer neighbors, the RDF of the first model diminishes faster at low and intermediate radial distance, where at $\sim$ 20– 250 Å, the RDF of the second model is generally larger than the first model. But the end point RDF of the second model is shorter.

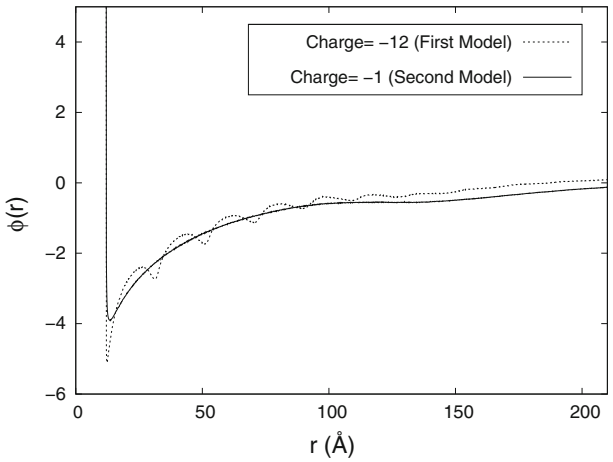

Fig. 12 The reduced electrostatic potential from two different DNA monomer models

This indicates that for the first model, the Na^+ ions is densely bound at the chain surface depleting the overall concentration elsewhere. At intermediate distances (i.e: $\sim$ 200–280 Å) the Na^+ concentration is relatively constant before tapering to zero. For the second model, the Na^+ concentration profile decreases slower at shorter distances compared to the first model but decrease faster at larger distances. In the second model, there is no indication of a plateau in the Na^+ concentration over the indicated range. The standard relationship between electrostatic potential (of mean force) $\psi(r)$ and the RDF is

$$g(r) = \frac{c_i(r)}{c_\infty} = e^{\frac{-z_i e\psi(r)}{kT}}, \tag{38}$$

where z_i, e, k, and T, are respectively the valence of the particle i, proton charge, Boltzmann constant and temperature. We convert the RDF data in Fig. 11 to the reduced potential $\phi(r)$ data in Fig. 12 where $\phi(r) = e\psi(r)/kT : \phi(r)$ describes the mean electrostatic potential at a distance r from any central charged monomer. As expected, from Fig. 12 we observe the fluctuations of the electrostatic potential for the first model which is not observed for the second model, as expected from the RDF's.

The axial distance between two nearest distant phosphate groups on opposite sides of the DNA thread is $\sim$ 1.7Å, and the nearest axial distance on the same side is 3.4Å. The experimental DNA cross-section is 20Å. If we represent the DNA as a string of bonded spheres, with the above dimensions, we would have the following topologies where all have the same charge (q/e) to bond length $(b/\text{Å})$ ratio, where topology X refers to X = {b, q} and in addition where b would represent the the diameter of the polymer thread. We define A = {20.4, −12}, B = {3.4, −2}, C = {1.7, −1}. Using the expression (27) given earlier, for $n = b$ to $n = s$ ($s = 6/2$ or 3 helical turns) for salt concentration c_s/mM, we have the following table of results [2, p. 43, Tab. 3.3] for the derived L_p values with the following settings ($L_p^0 = 500$Å, $l_B = 7.13$Å, $l_0 = 1$Å) for the same k_h and k_θ and other interaction parameters given earlier: The data in Table 2

Table 2 Table showing variation of L_p with topology

c_s	$L_p(A)$	$L_p(B)$	$L_p(C)$
100	601.91	559.24	554.10
10.0	778.5	617.34	603.95
1.0	888.91	646.05	628.03
0.1	933.51	656.55	636.78

shows that even for modeling the flexibility of the chain (let alone the potentials and concentration profiles in space), different choices of size and charge parameters that preserves a particular global variable like the charge density of the polyion with the same ff's leads to significant differences in the L_p variable, which characterizes flexibility. The above seems to indicate that whilst 'refinement' of models does lead to elucidation of structure [6], yet the choice of basic all-atom models that preserve global properties such as the charge densities still can give rise to different predicted physical properties and charge density distributions and thermodynamic state function values. Where distribution functions are concerned (such as RDF's), different models with different charge allocations [52, p. 207] on atomic sites for inorganic or small organometallic lattices and molecules could conceivably lead to different profiles based on the results presented here. For such systems, such variations may not be deemed significant, but for biological systems, perhaps changes of profiles would indeed be relevant, since this review shows that progress in the elucidation of biophysical phenomena is usually related to incorporation of greater detail. If this is to be the trend in the future, aided no doubt by greater computational power, then one might expect that broad ranging force-fields, like those developed by Jorgensen [55] would have to to be presented as a subset of many others, some specifically determined for the system of interest where the parameters cannot be provided by universal ff's. Many utilities, like the ATEN package [56] have a fixed set of such ff's for liquid state simulation, including OPLS that has to be manually modified, which can be tedious and impractical if used for MD of complex biophysical systems and organometallic lattices and zeolite lattices that contain fluid state molecules of polyelectrolytes. Such complex systems, such as the Cu-BTC metal-organic framework, the ff parameters have to be derived via DFT MD [57] (such as CPMD)[58]. There exists now an elaborate research program in supplying ff's for ionic liquid simulation [59–61] where the earlier softer ff's due to dispersive forces are not considered completely adequate. One might expect that a program for biological systems would be developed by matured and well developed research groups, such as that of Lavery and coworkers [62] for modeling requirements [63] where the computational methodology would require generating input parameters that are specific to the system of interest and where computational tools would be required for this input generation. Since the development of specialized ff's for IL and organometallic lattice simulations specific to the system is gradually becoming systematic [57], one could anticipate a similar trend to emerge in biophysical systems. Finally the snapshots in Fig. 10 and the shape profiles (Figs. 1–9) clearly depicts distinct topologies for the different ξ intensity parameter and ionic concentrations. It seems as if such elaborate topological structures are implied at the heart of much research

in catalysis, according to the reviews [64,65]. The impression in these reviews is that current research is motivated by practical considerations of determining the appropriate catalyst for reactions of commercial importance, which [65] focuses on, whereas [64] is more concerned with theory and general principles and applications of these principles. IL's have been described as having many functions over and beyond that of being a "green" solvent and as having a means of providing a "biphasic" environment, where the catalyst resides with the IL phase during the reaction [65, p. 3667] and the products and reactants in the other phase, leading to efficient separation of products and the catalyst; the term catalyst immobilization is associated with this phenomena. IL's share with polyelectrolytes an extended distribution of charges along a molecular backbone of high asymmetry (at the cationic species at least). The "acidity" of the IL with respect to the catalyst can be "tuned" based on the compositional ratio of the IL components. Clearly, electronic transfer processes, of such importance in catalytic activity is involved, but one suspects that the IL's also have a significant orientational role to play in supporting the catalyst. Whilst the review [65] is replete with chemical information, there is less discussion of topology and principles which is covered in greater detail by Hardacre et al. where some aspects of topology is mentioned, and these include (1) stabilization to agglomeration of both individual metallic nanoparticle catalyst and gold cluster nanoparticle by linkage to sulphonate terminated thiol IL (2) immobilization of IL in biphasic catalysis [64, p. 2620] (3) the use of IL's as templates to create complex structures (zeotype and other frameworks) [66] that have controlled catalytic functions [64, p. 2622]. If the DLVO theory [64, refs. 63–65 therein] has been used to account for some of the above interactions involving IL that is routinely used to account for biophysical system behavior [67] and polyelectrolyte systems, it seems almost inevitable that in time, the theoretical techniques developed to treat polyelectrolyte biophysical systems can be extended to tackle the problem of catalysis with IL's in lattice structures which can be viewed as a specialized polyelectrolyte whose orientational properties within the lattices contribute significantly in several ways to the specific catalytic phenomena. In our polyelectrolyte systems, we observe how changes in the value of the ξ variable leads to the formation of remarkably complex structures; such aspects of "tuning" are yet to be fully realized and exploited in the theory of catalysis.

5 Conclusion

For modest chain lengths, one can deduce various thermodynamical parameters over temperature; in the case of polyelectrolytes, we observe within just one isolated overall neutral polyelectrolyte system topological transition phenomena which can be exploited in applications, because of the various shape structures that are formed by non-bonding forces such as non-screened Coulombic forces; structures could be maintained without the impediment of bonds which might constrain the motion of external molecular species in a molecular assembly. Obviously such properties are of importance in chemical reaction dynamics and catalysis where the topology of the system is of importance in providing for a dynamical route in a chemical reaction with a lower activation energy; one can observe this phenomena concerning the shape of the simple

polyelectrolyte chain of this work; such observations and their implementation would allow for the design of charged systems that can form different shapes as desired in applications that are stabilized by the counterions externally. Before this feature can be exploited however, further systematic detailed study needs to be undertaken to understand how such designs can be implemented. Concerning phase transitions, these might be defined for simplistic models that often require infinite systems [68, van Hove, p. 403, Yang and Lee, p. 407] and a limited species of particle types with very elementary short range forces operating, as in the Ising model. For these systems, one might be able to deduce various critical exponents. Some have attempted to extend the concept of phase transitions by recourse to lattice (gas) models [68, p. 418, p. 436 (eqns. 5a-b)]. Then there are other models that presuppose discontinuity in second order derivatives and the possibility of invoking an order parameter, as in the Landau theory. Since biological systems are so much more complex, it would be best to keep an open view with regard to whether such phase transitions can be absolutely characterized by these theories that are useful for much simpler systems. Experimentally, DSC and other methods have been used to define the regime of transition phenomena [52, p. 60, Sect. 3.1.2.1]; in the same spirit, perhaps sharp transitions of certain thermodynamical variables like the specific heat or mean square fluctuation of energy variables in MD simulations that are largely non-synthetic might be utilized to tentatively characterize such systems. The presence of strong electrostatic interactions that is not so obviously apparent from classical equipartition does seem to indicate that such free energy differences (in particular that of Helmholtz and Gibbs') could be utilized for energy storage. Traditionally, in the field of electrochemistry, little attention has been paid to ionic molecular structure and energy changes associated with these structures under various charge intensity parameters; with the appropriate selection of coupled sub-assemblies and electrodes, these potential energies (due to structure) could be tapped electrochemically.

Finally, the distribution of particles are of importance in rationalizing biological activity [69] in MD simulations, but where the distribution functions are severely dependent on the type of model that is constructed. Since the current trend seems to be the incorporation of greater detail to the MD simulations to account for the experimental data, we may expect that specialized groups and their software would play a significant role in automation of ff's which are specific for the system so that the appropriate structural parameters and potentials for atomic simulations could be used unambiguously to validate experimental results.

Acknowledgments C.G.J would like to thank 1) C. Hardacre (School of Chemistry and Chemical Engineering) and J. Kohanoff (Atomistic Simulation Centre, School of Mathematics and Physics) both of QUB, Belfast for a congenial sabbatical environment where this was written and 2) Malaysian FRGS National Grant FP084/2010A and Univ. Malaya grant UMRG RG077/09AFR for funding.

References

1. C.G. Jesudason, A.P. Lyubartsev, A. Laaksonen, Conformational characteristics of a single flexible polyelectrolyte chain. EPJE **30**, 341–350 (2009)

2. A.A.J. Agung, Polyelectrolyte models and molecular dynamics studies of the DNA polymer and DNA-NCP complexes in salt solutions. M.Sc. Dissertation; Jesudason, C.G., Supervisor; University of Malaya (Science Faculty): Kuala Lumpur, Malaysia, (2011)
3. A.G. Cherstvy, Electrostatic interactions in biological DNA-related systems. PCCP **13**, 68–9942 (2011)
4. A.G. Cherstvy, Collapse of highly charged polyelectrolytes triggered by attractive dipole-dipole and correlation-induced electrostatic interactions. J. Phys. Chem. B **114**, 5241–9 (2010)
5. A.G. Cherstvy, Effect of a low-dielectric interior on DNA electrostatic response to twisting and bending. J. Phys. Chem. B **111**, 12933–12937 (2007)
6. A.G. Cherstvy, R. Everaers, Layering, bundling, and azimuthal orientations in dense phases of nucleosome core particles. J. Phys. Condens. Matter **18**, 11429–11442 (2006)
7. N. Korolev, A.P. Lyubartsev, L. Nordenskiold, Application of polyelectrolyte theories for analysis of DNA melting in the presence of Na^+ and Mg^{2+} ions. Biophys. Chem. **75**, 3041–3056 (1998)
8. N. Korolev, A.P. Lyubartsev, A. Laaksonen, Electrostatic background of chromatin fiber stretching. J. Biomol. Struct. Dyn. **22**, 215–226 (2002)
9. D. Stigter, Evaluation of the counterion condensation theory of poly-electrolytes. Biophys. J. **69**, 380–388 (1995)
10. J. Jeon, A.V. Dobrynin, Necklace globule and counterion condensation. Macromolecules **40**, 7695–7706 (2007)
11. R. Kumar, G.H. Fredrickson, Theory of polyzwitterion conformations. J. Chem. Phys. **131**, 104901 (2009)
12. K.K. Kunze, R.R. Netz, Salt-induced DNA-histone complexation. PRL **85**, 92–4389 (2000)
13. Q. Liao, A.V. Dobrynin, M. Rubinstein, C. Hill, N. Carolina, Counterion-correlation-induced attraction and Necklace formation in polyelectrolyte solutions: theory and simulations. Macromolecules **39**, 1920–1938 (2006)
14. G.S. Manning, The interaction between a charged wall and its counterions: a condensation theory. J. Phys. Chem. B **114**, 5435–40 (2010)
15. S.G. Walker, C.J. Dale, A. Lyddiatt, G.S. Manning, Counterion condensation theory constructed from different models. Physica A **231**, 236–253 (1996)
16. G.S. Manning, Limiting laws and counterion condensation in polyelectrolyte solutions I. Colligative properties. J. Chem. Phys. **51**, 924–933 (1969)
17. M. Muthukumar, Adsorption of a polyelectrolyte chain to a charged surface. J. Chem. Phys. **86**, 7230–35 (1987)
18. M. Muthukumar, Theory of counter-ion condensation on flexible polyelectrolytes: adsorption mechanism. J. Chem. Phys. **120**, 9343–9350 (2004)
19. P. Loh, G.R. Deen, D. Vollmer, K. Fischer, M. Schmidt, A. Kundagrami, M. Muthukumar, Collapse of linear polyelectrolyte chains in a poor solvent: when does a collapsing polyelectrolyte collect its counterions? Macromolecules **41**, 9352–9358 (2008)
20. A. Kundagrami, M. Muthukumar, Effective charge and coil-globule transition of a polyelectrolyte chain. Macromolecules **43**, 2574–2581 (2010)
21. Z. Ou, M. Muthukumar, Entropy and enthalpy of polyelectrolyte complexation: Langevin dynamics simulations. J. Chem. Phys. **124**, 154902(1–11) (2006)
22. R. Winkler, M. Gold, P. Reineker, Collapse of polyelectrolyte macromolecules by counterion condensation and ion pair formation: a molecular dynamics simulation study. PRL **80**(17), 3731–3734 (1998)
23. R. Winkler, M. Steinhauser, P. Reineker, Complex formation in systems of oppositely charged polyelectrolytes: a molecular dynamics simulation study. Phys. Rev. E **66**, 021802 (2002)
24. A.A. Kornyshev, S. Leikin, Theory of interaction between helical molecules. J. Chem. Phys. **107**, 3656–74 (1997)
25. A. Kornyshev, D. Lee, S. Leikin, A. Wynveen, Structure and interactions of biological helices. Rev. Mod. Phys. **79**(3), 943–996 (2007)
26. T. Nguyen, B. Shklovskii, Persistence length of a polyelectrolyte in salty water: Monte Carlo study. Phys. Rev. E **66**, 021801 (2002)
27. A.P. Lyubartsev, L. Nordenskiöld, Monte Carlo simulation study of DNA polyelectrolyte properties in the presence of multivalent polyamine ions. J. Phys. Chem. B **101**, 4335–4342 (1997)
28. A.P. Lyubartsev, L. Nordenskiöld, Computer simulations of polyelectrolytes, in *Handbook of Polyelectrolytes and Their Applications, vol 3. Applications of Polyelectrolytes and Theoretical Models*,

ed. by S.K. Tripathy, J. Kumar, H.S. Nalwa (American Scientific Publishers, California, USA, 2002), pp. 309–326. Chap. 11
29. N.A. Volkov, P.N. Vorontsov-Velyaminov, A.P. Lyubartsev, Entropic sampling of flexible polyelectrolytes within the Wang-Landau algorithm. Phys. Rev. E **75**, 016705-(1–10) (2007)
30. R.H. French, R. Podgornik, R.F. Rajter, A. Jagota, J. Luo, D. Asthagiri, M.K. Chaudhury, Y. Chiang, S. Granick, S. Kalinin, M. Kardar, R. Kjellander, D.C. Langreth, J. Lewis, S. Lustig, D. Wesolowski, J.S. Wettlaufer, W. Ching, M. Finnis, F. Houlihan, O.A. von Lilienfeld, C.J. van Oss, T. Zemb, Long range interactions in nanoscale science. Rev. Mod. Phys. **82**, 1887–1944 (2010)
31. S. Leikin, V.A. Parsegian, D.C. Rau, Hydration forces. Annu. Rev. Phys. Chem. **44**, 369–395 (1993)
32. Y. Hayashi, M. Ullner, P. Linse, Complex formation in solutions of oppositely charged polyelectrolytes at different polyion compositions and salt content. J. Phys. Chem. B **107**, 8198–8207 (2003)
33. Y. Hayashi, M. Ullner, P. Linse, A Monte Carlo study of solutions of oppositely charged polyelectrolytes. J. Chem. Phys. **116**(15), 6836–6845 (2002)
34. P. Linse, Simulation of charged colloids in solution. Adv. Polym. Sci. **185**, 111–162 (2005)
35. M. Ullner, C.E. Woodward, Orientational correlation function and persistence lengths of flexible polyelectrolytes. Macromolecules **35**, 1437–1445 (2002)
36. P.N. Vorontsov-Velyaminov, N.A. Volkov, A.A. Yurchenko, Entropic sampling of simple polymer models within Wang-Landau algorithm. J. Phys. A **37**, 1573–1588 (2004)
37. J. Klos, T. Pakula, Lattice Monte Carlo simulations of three-dimensional charged polymer chains. J. Chem. Phys. **120**(5), 2496–2501 (2004)
38. H. Limbach, A. Arnold, B.A. Mann, C. Holm, ESPResSo—an extensible simulation package for research on soft matter systems. Comput. Phys. Commun. **174**(9), 704–727 (2006)
39. M. Deserno, C. Holm, How to mesh up Ewald sums. I. A theoretical and numerical comparison of various particle mesh routines. J. Chem. Phys. **109**(18), 7678–7693 (1998)
40. H.J.C. Berendsen, J.P.M. Postma, W.F. van Gunsteren, A. DiNola, J.R. Haak, Molecular dynamics with coupling to an external bath. J. Chem. Phys. **81**(8), 3684–3690 (1984)
41. B.Y. Ha, D. Thirumalai, Electrostatic persistence length of a polyelectrolyte chain. Macromolecules **28**, 577–581 (1995)
42. A.Y. Grosberg, A.R. Kholkhlov, *Statistical physics of macromolecules* (AIP Press, New York, USA, 1994)
43. T. Odijk, Polyelectrolytes near the rod limit. J. Poly. Sci. Poly. Phys. Ed. **15**, 477–483 (1977)
44. J. Skolnick, M. Fixman, Electrostatic persistence length of a wormlike polyelectrolyte. Macromolecules **10**, 944–948 (1977)
45. A.V. Dobrynin, Electrostatic persistence length of semiflexible and flexible polyelectrolytes. Macromolecules **38**, 9304–9314 (2005)
46. G.S. Manning, The persistence length of DNA is reached from the persistence length of Its null isomer through an internal electrostatic stretching force. Biophys. J. **91**, 3607–3616 (2006)
47. B.S. Smith, L. Finzi, C. Bustamante, Direct mechanical measurements of the elasticity of single DNA molecules by using magnetic beads. Science **258**, 1122–1126 (1992)
48. E. Nordmeier, Absorption and dynamic and static light-scattering studies of ethidium bromide binding to Calf Thymus DNA: implications for outside binding and intercalation. J. Phys. Chem. **96**, 6045–6055 (1992)
49. C. Baumann, B.S. Smith, A.V. Bloomfield, C. Bustamante, Ionic effect on the elasticity of single DNA molecules. Proc. Natl. Acad. Sci. USA **94**, 6185–6190 (1997)
50. V. Rizzo, J.A. Schellman, Flow dichroism of T7 DNA as a function of salt concentration. Biopolymers **20**, 2143–2163 (1981)
51. I.T. Todorav, W. Smith, THE DL_POLY_MANUAL; Version 4.03.4; STFC Daresbury Laboratory. (Daresbury, UK, 2012, June)
52. P. Hunt, E.J. Maginn, R.M. Lynden-Bell, M.G. Del Popolo, Computational modeling of ionic liquids, in *Ionic Liquids in Synthesis*, vol. 1, ed. by P. Wasserscheid, T. Welton (Darmstadt, Germany, 2008), pp. 206–249
53. D.F. Evans, H. Wennerström, *The Colloidal Domain*, 2nd edn. (Wiley-VCH, New York, USA, 1999)
54. C.G. Jesudason, Model hysteresis dimer molecule II: deductions from probability profile due to system coordinates. JOMC **42**(14), 893–908 (2007)
55. W.L. Jorgensen, D.S. Maxwell, J. Tirado-Rives, Development and testing of the OPLS all-atom force field on conformational energetics and properties of organic liquids. J. Am. Chem. Soc. **118**(45), 11225–11236 (1996)

56. T.G.A. Youngs, Aten—An application for the creation, editing, and visualization of coordinates for glasses, liquids, crystals, and molecules. J. Comput. Chem. **31**, 639–648 (2009)
57. L. Zhao, Q. Yang, Q. Ma, C. Zhong, J. Mi, D. Liu, A force field for dynamic Cu-BTC metal-organic framework. J. Mol. Model. **17**, 227–234 (2011)
58. R. Car, M. Parrinello, Unified approach for molecular dynamics and density-functional theory. PRL **55**(22), 2471–2474 (1985)
59. N. Canongia Lopes, J. Deschamps, A.A.H. Padua, Modeling ionic liquids using a systematic all-atom force field. J. Phys **108**, 2038–2047 (2004)
60. M.S. Kelkar, W. Shi, E.J. Maginn, Determining the accuracy of classical force fields for ionic liquids: atomistic simulation of the thermodynamic and transport properties of 1-Ethyl-3-methylimidazolium ethylsulfate ([emim][$EtSO_4$]) and its mixtures with water. Ind. Eng. Chem. Res. **47**, 9115–9126 (2008)
61. N. Canongia Lopes, J. Deschamps, A.A.H. Padua, Molecular force field for ionic liquids IV: trialkylimidazolium and alkoxycarbonyl-Imidazolium cations; alkylsulfonate and alkylsulfate anions. J. Phys. Chem. B **112**, 5039–5046 (2008)
62. M. Wilhelm, A. Mukherjee, B. Bouvier, K. Zakrzewska, J.T. Hynes, R. Lavery, Multistep drug intercalation: molecular dynamics and free energy studies of the binding of daunomycin to DNA. J. Am. Chem. Soc. **134**, 8588–8596 (2012)
63. S. Sacquin-Mora, R. Lavery, Modeling the mechanical response of proteins to anisotropic deformation. Chem. Phys. Chem. **10**, 115–118 (2009)
64. V.I. Parvulescu, C. Hardacre, Catalysis in ionic liquids. Chem. Rev. **107**, 2615–2665 (2007)
65. J. Dupont, R.F. de Souza, P.A.Z. Suarez, Ionic liquid (molten salt) phase organometallic catalysis. Chem. Rev. **102**, 3667–3692 (2002)
66. R.A.A. Melo, M.V. Giotto, J. Rocha, E.A. Urquieta-González, MCM-41 ordered mesoporous molecular sieves synthesis and characterization. Mater. Res. **2**, 173–179 (1999)
67. A.J. de Kerchove, P. Weronski, M. Elimelech, Adhesion of nonmotile pseudomonas aeruginosa on "Soft" polyelectrolyte layer in a radial stagnation point flow system: measurements and model predictions. Langmuir **23**, 12301–12308 (2007)
68. R.K. Pathria, P.D. Beale, *Statistical Mechanics*, 1st edn. (Elsevier, Amsterdam, 2011)
69. N. Korolev, A.P. Lyubartsev, L. Nordenskiöld, Computer modeling demonstrates that electrostatic attraction of nucleosomal DNA is mediated by histone tails. Biophys. J. **90**, 4305–4316 (2006)